Pergamon

Ultrasound in Med. & Biol., Vol. 20, No. 5, pp. 403–428, 1994

0301-5629/94 $6.00 + .00

0301-5629(94)E0009-2

●*Review*

BIOMEDICAL ULTRASOUND BEAM FORMING

JIAN-YU LU, HEHONG ZOU and JAMES F. GREENLEAF
Biodynamics Research Unit, Department of Physiology and Biophysics, Mayo Clinic and Foundation, Rochester, MN 55905, USA

(*Received and in final form* 20 *October* 1993)

Abstract—The principles of biomedical ultrasound beam forming control the quality of diagnostic imaging. Beam parameters associated with imaging quality are: (1) lateral and axial resolutions; (2) depth of field; (3) contrast and (4) frame rate. In this paper, we review some of the current beam forming techniques and their principles. We focus on trade-offs among the above four aspects of beam forming and relate them to system parameters such as aperture size, *f*-number (the ratio between focal length and aperture diameter), central frequency (wavelength), system bandwidth and sidelobes. Methods for steering conventional and limited diffraction beams with array transducers are also reviewed.

Key Words: **Arrays, Bandwidth, Beam forming, Focused beams, Gaussian beams, Grating lobes, Imaging, Limited diffraction beams, Localized waves, Nondestructive evaluation, Scan, Sidelobes, Steering, Subluminal, Subsonic, Superluminal, Tissue characterization, Ultrasonic transducers, Unweighted beams, Weighted beams.**

INTRODUCTION

Beam-forming technique plays one of the most important roles in ultrasonic imaging. In this paper, we review some of the current conventional beams and recently developed limited diffraction beams, and describe the trade-offs among some beam parameters, such as resolution, sidelobes, frame rate, central frequency, bandwidth, aperture and depth of field. The main difference between these two types of beams is that the former usually focuses at a fixed or varying point, while the latter tend to focus in a line along their propagation direction.

Conventional focused beams have lower sidelobes within the range of a short depth of field. Away from this range, images obtained may blur quickly due to the increase of the lateral beamwidth. One effective way to increase the depth of field while maintaining the low sidelobes is to use dynamically focused reception, which increases the focal length of the receiving beam electronically with time, so that echoes returned from all depths within the tissue are continuously in focus. The idea of dynamic focusing can also be applied to transmission of beams to further increase the depth of field by transmitting several pulse sequences, each of which focuses at a different point. Obviously this process improves the imaging quality but reduces the frame rate significantly.

In contrast to conventional beams, limited diffraction beams have large depth of field, good focus, but high sidelobes. The deep depth of field is paid for by high sidelobes. The high sidelobes can be suppressed by subtracting different types of beams that have no central lobes but similar sidelobes. Thus, low sidelobes can be obtained with limited diffraction beams but at the expense of frame rate. However, using both limited diffraction transmission and conventional dynamically focused reception in pulse-echo imaging may combine the advantages of the two types of beams to produce high frame rate, large depth of field and low sidelobe images (Lu et al. 1993).

This paper is organized as follows: in the next section, we begin by reviewing some of the conventional beam-forming techniques. Trade-offs of different aspects of beam forming are also discussed. Next, theory and production of limited diffraction beams will be reviewed by deriving a general class of special solutions to the isotropic/homogeneous scalar wave equation. Techniques for sidelobe reduction will also be discussed. Methods of beam steering are summarized next. Finally, a brief discussion and conclusion will be made.

Address correspondence to: Jian-Yu Lu.

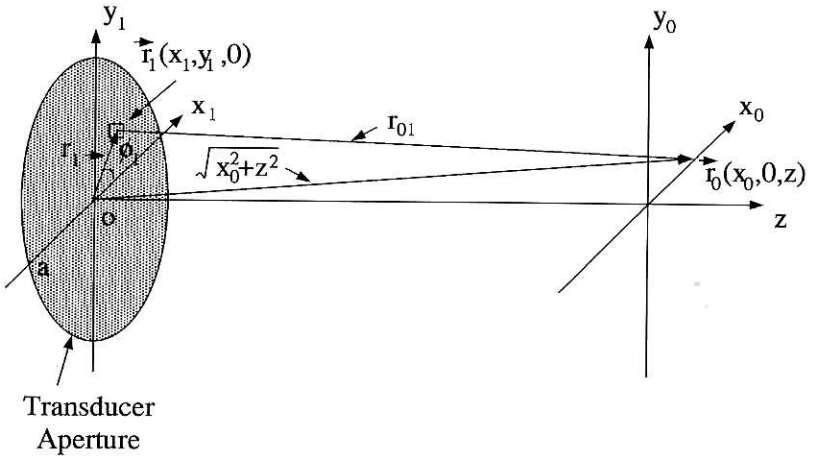

Fig. 1. Coordinate system used for eqn (1) to calculate fields in space. Wave sources are located in the plane, $z = 0$. Fields are calculated at $\vec{r}_0 = \vec{r}_0(x_0, y_0, z)$. Modified with permission from Fig. B-1 of Lu and Greenleaf 1993b. © 1993 IEEE.

CONVENTIONAL BEAM FORMING

The study of beam forming began in 1678 by Huygens, who gave an intuitive postulation of beam formation using wavelets. This postulation was improved by Fresnel in 1818 with a quantitative description. Later, more accurate formulas such as the Rayleigh–Sommerfeld diffraction formula were developed in optics. In this section, we review the basic concepts of various conventional beam-forming techniques. Discussions can be found in Goodman's and Kino's books (Goodman 1968; Kino 1987).

Rayleigh–Sommerfeld diffraction formula

Basic principles of beam forming are given by the Rayleigh–Sommerfeld diffraction formula that was developed in optics (Goodman 1968). The formula can accurately predict the field (pressure or velocity potential) at any spatial point, $\vec{r}_0 = (x_0, y_0, z)$, produced by a finite aperture (Fig. 1). Specifically, suppose the aperture is a disc with radius a, then we have

$$\tilde{\Phi}(\vec{r}_0, \omega) = \frac{1}{i\lambda}\int_0^a\int_{-\pi}^{\pi}\tilde{\Phi}(\vec{r}_1, \omega)e^{ikr_{01}}\frac{z}{r_{01}^2}r_1 dr_1 d\phi_1 + \frac{1}{2\pi}\int_0^a\int_{-\pi}^{\pi}\tilde{\Phi}(\vec{r}_1, \omega)e^{ikr_{01}}\frac{z}{r_{01}^3}r_1 dr_1 d\phi_1, \quad (1)$$

where the first and second terms represent high and low frequency contributions, respectively, a transducer is located at the plane, $z = 0$, $\tilde{\Phi}(\vec{r}_0, \omega)$ is the Fourier transform of the wave field, $\Phi(\vec{r}_0, t)$, at the spatial point $\vec{r}_0$, $\tilde{\Phi}(\vec{r}_1, \omega)$ denotes the Fourier transform of a complex aperture weighting function, $\Phi(\vec{r}_1, t)$, applying at a source point $\vec{r}_1 = (x_1, y_1, 0)$ on the surface of the transducer, $r_1 = \sqrt{x_1^2 + y_1^2}$, $\phi_1 = \tan^{-1}(y_1/x_1)$, λ is wavelength, $\omega = 2\pi f_0$ is angular frequency, where f_0 is frequency, $k = 2\pi/\lambda = \omega/c$ denotes the wave number, where c is the speed of wave in the medium, and r_{01} is the distance between the field point $\vec{r}_0$ and the source point $\vec{r}_1$, which is given by

$$r_{01} = \sqrt{(x_0 - x_1)^2 + (y_0 - y_1)^2 + z^2}. \quad (2)$$

Equation (1) involves two double integrals. Therefore, its computation is usually time consuming. Efforts have been devoted to simplify eqn (1) under certain conditions. Note that when $r_{01} \gg \lambda/(2\pi)$, which is usually satisfied in practical beam forming, the second term in eqn (1) is negligible. Furthermore, in the Fresnel region where r_1 and $r_0 \ll \sqrt{r_0^2 + z^2}$, and where $r_0 = \sqrt{x_0^2 + y_0^2}$, for some aperture weighting functions of $\tilde{\Phi}(\vec{r}_1, \omega)$, the double integration in eqn (1) can be simplified to a single one by using the Fresnel approximation (Goodman 1968). In the far field (Fraunhofer region) of the transducer, where $r_{01} \approx z$, and $z \gg kr_1^2/2$, the field is related to the Fourier transform of the transducer aperture (Goodman 1968). For some special aperture weighting functions such as the uniform functions with or without focusing, a simplified formula for eqn (1) can be obtained without using the Fresnel or Fraunhofer approximation (Lin et al. 1989).

Conventional beams

Unfocused piston transducer. The simplest ultrasonic transducer is an unfocused piston transducer

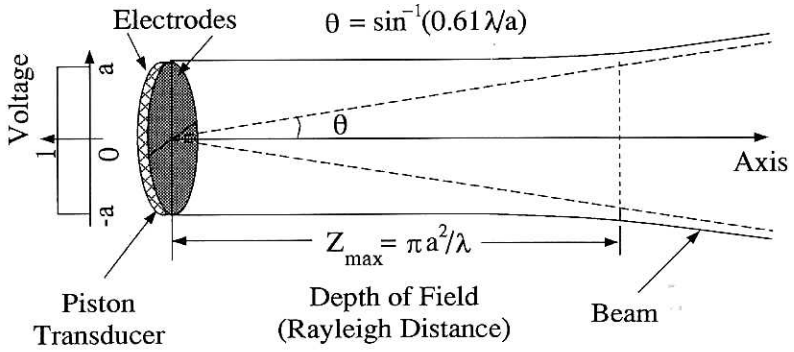

Fig. 2. A beam produced with a piston transducer. The beam has little spreading within the Rayleigh distance and has a beamwidth about as wide as the diameter of transducer $D = 2a$. The whole aperture of the transducer is excited by the same voltage (no weighting). After the Rayleigh distance, the beam spreads out at an angle $\theta = \sin^{-1}(0.61\lambda/a)$.

(Fig. 2) that consists of a piezoelectric disc with thin electrodes deposited on both sides of the disc. Electrical signals are applied to or produced from the electrodes. The transducer is uniformly weighted (unweighted, $\tilde{\Phi}(\vec{r}_1, \omega) \equiv 1$ in eqn (1)) and its surfaces vibrate like an engine piston when excited by an electrical signal. The main beamwidth produced by this transducer is approximately the same as the diameter of the transducer, D, in the depth of field that is defined as the Rayleigh distance (Durnin et al. 1987)

$$PZ_{\max} = \frac{\pi a^2}{\lambda}, \tag{3}$$

where a and λ denote the radius and central wavelength of the transducer. At the Rayleigh distance, the amplitude of field pressure drops to about one half of that on the transducer surface (Wells 1977).

In the far field where the Fraunhofer approximation is valid, the lateral field pattern (Airy pattern) of the beam produced by the unfocused piston transducer is proportional to the Fourier transform of the aperture (assumed to be a disc) of the transducer and can be derived from eqn (1) as (Goodman 1968)

$$\tilde{\Phi}(\vec{r}_0, \omega) = \frac{ka^2}{i2z} e^{ik(z - r_0^2/2z)} \left[2 \frac{J_1(kar_0/z)}{kar_0/z} \right], \tag{4}$$

where $J_1(\cdot)$ is the first-order Bessel function of the first kind. The first minimum of $|\tilde{\Phi}(\vec{r}_0, \omega)|$ along the radius is at

$$r_0 = 0.61 \frac{\lambda z}{a}. \tag{5}$$

Equation (5) represents half of the main beamwidth of the unfocused piston transducer. Hence the main beamwidth increases with the axial distance, z, for a given central wavelength, λ, and decreases as the size of aperture of the transducer, a, increases. The beam spreading is the result of wave diffraction.

Focused piston transducer. Consequently, the lateral beamwidth of the above unfocused piston transducer is very large and the lateral resolution of the images obtained with such a transducer is low. The main beamwidth of a piston transducer, equivalently the lateral resolution of images, can be greatly improved if the spherical-focusing technique in optics is applied. The field of a focused piston transducer can be calculated by eqn (1) with the following aperture weighting function that is a spherical phase shifter along the radial distance, r_1:

$$\tilde{\Phi}(\vec{r}_1, \omega) = e^{-ik(\sqrt{F^2 + r_1^2} - F)}, \tag{6}$$

where F is the focal length of the transducer. Under the Fresnel approximation, one obtains the field in the focal plane from eqn (1) (Goodman 1968)

$$\tilde{\Phi}(\vec{r}_0, \omega) \propto \left[2 \frac{J_1(kar_0/F)}{kar_0/F} \right], \tag{7}$$

where the first minimum of $|\tilde{\Phi}(\vec{r}_0, \omega)|$ along the radius is at

$$r_0 = 0.61 \frac{\lambda F}{a} = 1.22\lambda f, \tag{8}$$

in which $f = F/(2a)$ is defined as an f-number. It implies

that the main beamwidth increases with the f-number for a given central wavelength. Hence, a beam cannot be properly focused with a larger f-number or the lateral resolution cannot be improved by focusing a beam with a focal length that is in the Fraunhofer region, where eqns (5) and (8) are identical.

Focused Gaussian-weighted transducer. Although a focused piston transducer can reduce the beamwidth at its focus, its sidelobes are not reduced (compare eqns (4) and (7)). To suppress the sidelobes, various forms of the aperture weighting function, $\tilde{\Phi}(\vec{r}_1, \omega)$, of eqn (1) can be applied. As an example,

$$\tilde{\Phi}(\vec{r}_1, \omega) = e^{-r_1^2/\sigma^2 - ik(\sqrt{F^2+r_1^2}-F)} \tag{9}$$

gives a focused Gaussian-weighted beam. In this case, the field distribution (either the pressure or velocity potential) on the surface of the transducer is a Gaussian function $e^{-r_1^2/\sigma^2}$, where σ denotes the radius at which the field amplitude drops to $1/e$ of its maximum. The Gaussian weighted beam can also be characterized by the full width at half maximum (FWHM) of the Gaussian function at the transducer surface. The FWHM is related to σ by

$$\text{FWHM}_{\text{FG}|z=0} = 2\sqrt{\ln 2}\sigma \approx 1.67\sigma, \tag{10}$$

where "FG" stands for focused Gaussian. Under both the Fresnel approximation and paraxial condition (field observed is not too far away from the axis), the lateral profile of a Gaussian beam (assume that $\sigma^2 \ll a^2$) in the focal plane is still proportional to a Gaussian function (Lu and Greenleaf 1990b), e.g.,

$$\tilde{\Phi}(\vec{r}_0, \omega) \propto e^{-r_0^2 \Big/ \left(\frac{\lambda F}{\pi\sigma}\right)^2}. \tag{11}$$

The Gaussian beam specified by eqn (11) has lower sidelobes because the Gaussian function approaches zero faster as the radial distance increases.

Similar to the beam produced by a focused piston transducer, the Gaussian beam can not be properly focused if

$$F > \frac{\pi\sigma^2}{\lambda}, \tag{12}$$

where $\pi\sigma^2/\lambda$ is called the Rayleigh distance of an unfocused Gaussian beam and σ is called the effective radius of the aperture. From eqn (11), it is obvious that the beamwidth at $z = F = \pi\sigma^2/\lambda$ is the same as that at the transducer surface (eqn (9)).

Because $\sigma < a$, the effective aperture size of the Gaussian transducer is smaller than that of the piston transducer with the same radius, a. The reduced effective aperture size of the Gaussian transducer increases the FWHM of the beam in the focal plane. Therefore, the lower sidelobes gained by the Gaussian beam are at the expense of the larger lateral beamwidth (or lower lateral imaging resolution). However, because the Gaussian transducer has a lower field amplitude at its edge than the piston transducer, edge waves are lower in the Gaussian beam than in the piston beam. (Edge waves are produced by an abrupt truncation of the field at the edges of transducers. They exist everywhere in some transducer geometries except at the foci of beams and might cause ghosts in imaging (Krautkramer and Krautkramer 1975).)

Trade-offs between lateral beamwidth and depth of field

For analytical simplicity and without the loss of generality, the focused Gaussian beam is used for studying the trade-offs between the lateral beamwidth and depth of field. If the depth of field of the focused Gaussian beam is defined as the distance between two out-of-focus planes in which the beamwidths increase to $\sqrt{2}$ times that in the focal plane (Fig. 3), we have (Kino 1987; Lu and Greenleaf 1990b)

$$GZ_{\max} = 2\frac{\sqrt{\frac{\sigma^4}{F^2} - \left[\left(\frac{2}{k\sigma}\right)^2 + \left(\frac{\sigma}{F}\right)^2\right]\left[\sigma^2 - 8\left(\frac{F}{k\sigma}\right)^2\right]}}{\left(\frac{2}{k\sigma}\right)^2 + \left(\frac{\sigma}{F}\right)^2}, \tag{13}$$

where F must be so small that the above two out-of-focus planes exist simultaneously ($z \geq 0$ must be satisfied for the out-of-focus planes), *i.e.,*

$$F \leq \frac{1}{\sqrt{2}}\frac{\pi\sigma^2}{\lambda}. \tag{14}$$

Neglecting the term, $(2/(k\sigma))^2$, in the denominator of eqn (13), one obtains

$$GZ_{\max} \approx 2\left(\frac{\lambda F^2}{\pi\sigma^2}\right)\sqrt{1 + 2\left(\frac{\lambda F}{\pi\sigma^2}\right)^2}. \tag{15}$$

On the other hand, from eqn (11) the FWHM of the

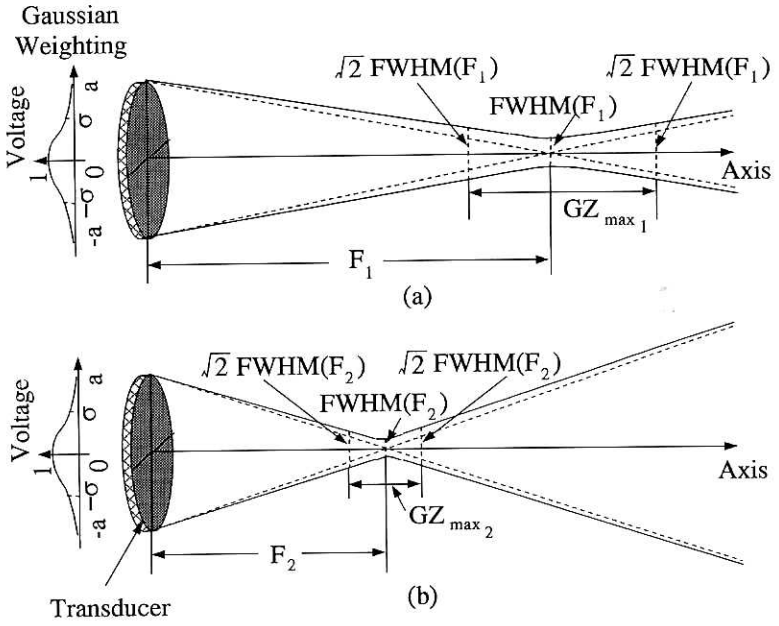

Fig. 3. Focused Gaussian beams produced with Gaussian aperture weighting. With the same effective radius of aperture, σ, a shorter focal length produces a beam of a smaller beamwidth at focus, but has a shorter depth of field.

Gaussian beam at focus becomes

$$\mathrm{FWHM}_{\mathrm{FG}|z=F} = \left(\frac{2}{\pi}\sqrt{\ln 2}\right)\frac{\lambda F}{\sigma} \approx 0.53\,\frac{\lambda F}{\sigma}. \quad (16)$$

Trade-offs between the lateral beamwidth (lateral imaging resolution) in the focal plane of a focused Gaussian beam and the depth of field are demonstrated by eqns (15) and (16). In particular, for a given central wavelength, λ, to increase the lateral resolution (reduce FWHM in the focal plane), the effective f-number, F/σ, must be reduced. However, this reduces the depth of field. Furthermore, for a given effective f-number, the diffraction of Gaussian beam is stronger as the central wavelength increases. This lowers the lateral imaging resolution but increases the depth of field.

Therefore, to obtain higher resolution in diagnostic ultrasound imaging, high frequency (small central wavelength) is desirable. However, the highest frequency used must be limited by the penetration depth of ultrasound in biological soft tissues in which higher frequencies have larger attenuation.

Increasing depth of field

Dynamically focused reception. When the Fresnel approximation, paraxial condition, and $\sigma^2 \ll a^2$ are satisfied, the FWHM of a focused Gaussian beam at distance, z, is given by (Lu and Greenleaf 1990b)

$$\mathrm{FWHM}_{\mathrm{FG}|z=z} = 2\sqrt{\ln 2}\sqrt{\left(\frac{2z}{k\sigma}\right)^2 + \left(\frac{\sigma}{F}\right)^2 (z-F)^2}. \quad (17)$$

The above equation infers that the lateral beamwidth varies with both z (first term) and the off-focus distance, $|z - F|$ (second term), and that the FWHM reaches a minimum at $z = [1/(1 + (F\lambda/(\pi\sigma^2))^2)]F < F$. To focus effectively, F must be much less than $\pi\sigma^2/\lambda$. In this case, $z \approx F$ and eqn (17) is identical to eqn (16).

One effective way to increase the depth of field in biomedical diagnostic imaging without sacrificing the lateral beamwidth is called dynamically focused reception (Fig. 4), in which the focal length of an array transducer receiving system is changed with time so

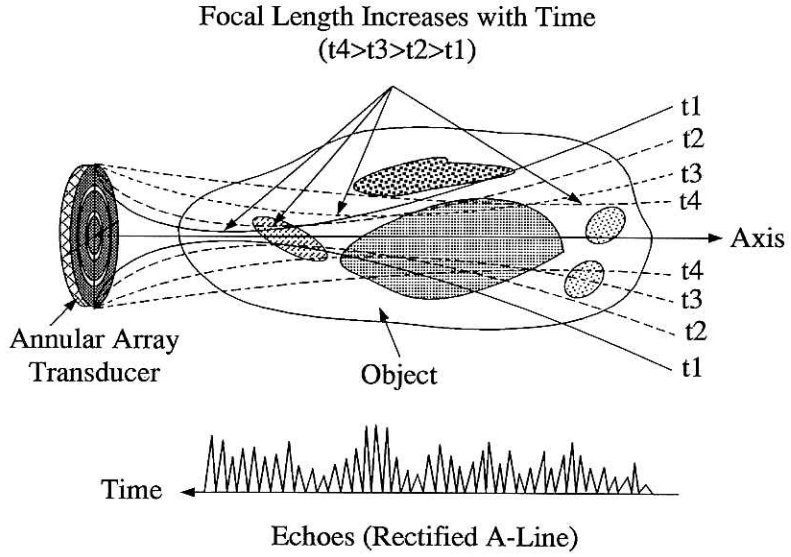

Fig. 4. Schematic of dynamic focusing in reception. The focal length of a transducer is increased with time so that echoes from various depths are in focus.

that echoes from all depths are always in focus. This process is equivalent to keeping $z \approx F$ for all F and obtaining the minimum FWHM (or highest lateral resolution) in imaging over a large depth of field.

When $z \approx F$, the lateral beamwidth changes linearly with F or z (eqn (16)). If the depth of field for the dynamically focused reception is defined as the distance between the two planes in which the beamwidth at focus is decreased or increased by $\sqrt{2}$, we obtain

$$GZ^{D}_{\max} = F/\sqrt{2}, \tag{18}$$

where the superscript "D" means dynamic focusing and F is a reference focal length. The depth of field given by eqn (18) is much larger than that calculated from eqn (13). For example, if $F = 120$ mm, we have $GZ^{D}_{\max} = 84.85$ mm. In contrast, if $\lambda = 0.6$ mm and $\sigma = 15$ mm, the depth of field calculated from eqn (13) is only 24.44 mm for the same F.

Because of the above reasons, dynamically focused reception has been widely used in modern commercial diagnostic imaging equipment. Because the change of focal length in reception can be done electronically in real-time, the process does not reduce imaging frame rate.

Dynamically focused transmission. The same dynamic focusing idea can also be applied to transmission of beams. It can be shown that the lateral resolution of images can be further improved, and the sidelobes of beams further suppressed, if dynamic focusing is used in both transmission and reception. This advantage is due to the fact that the lateral beam profile of a transmission-reception (pulse-echo) system is the product of the profiles of transmission and of reception.

The disadvantage of this approach is that beams of different focal lengths can only be transmitted one by one, and retransmission of the second beam must wait until all echoes produced by the previous one return to the transducer. Otherwise, echoes produced from the second beam coming from shallower tissues may arrive at the same time as those produced by the first beam coming from deeper tissues, thus producing a false representation of structures in imaging.

Dynamically focused transmission is performed with a montage process where images obtained with different transmission focal lengths are cut around their focal lengths and mounted next to each other to form a new frame of image (Fig. 5). It is obvious that this process increases the time to form a frame of image. Montage using an infinite number of images obtained around all focal depths would produce an image of the highest quality, however, this would require an infinite amount of time and have a zero imaging frame rate. Therefore, in practice, one needs to consider the trade-off between the quality of images and the frame rate. In cardiac imaging, dynamically focused transmission is usually not used because of the need for high frame rate.

Ring transducer. Another way to increase the

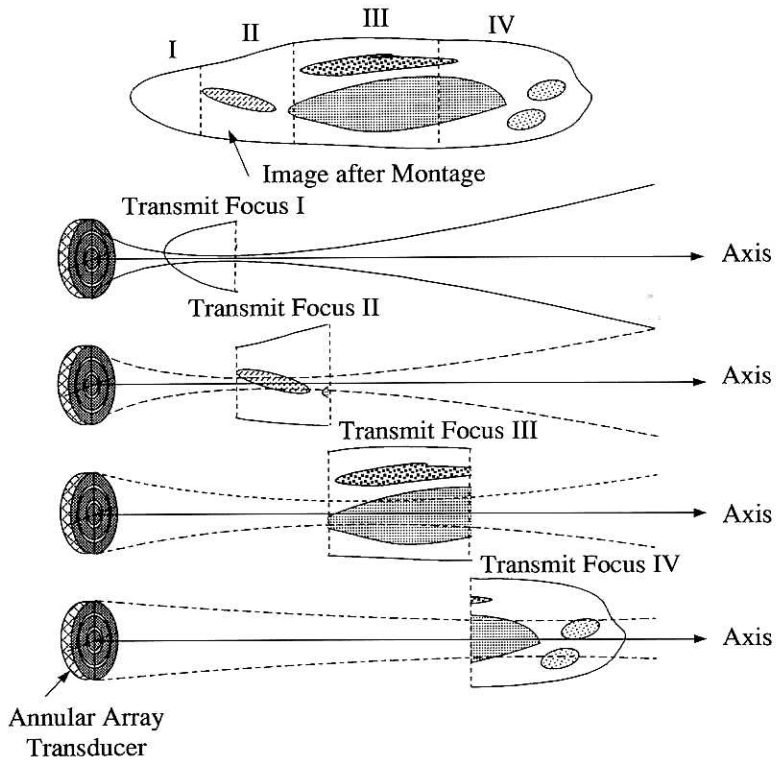

Fig. 5. The montage process that is used in ultrasound scanners for medical imaging. Images obtained with different transmission foci are cut and mounted next to each other to form an image with large depth of field. This process reduces imaging frame rate.

depth of field is to simply use a ring transducer (a thin ring) (Wild, 1965; Burkhardt et al. 1973a). On the axis near the source plane where the ring transducer is located, the field distribution in the lateral direction is complex and the field has no central maximum. However, in the Fraunhofer region (far field), the field in the lateral direction is proportional to the Fourier transform of the transducer aperture (a ring) and has a central maximum. The aperture weighting function of a ring transducer can be defined as

$$\tilde{\Phi}(\tilde{r}_1, \omega) = \delta(r_1 - a), \tag{19}$$

where δ is a Dirac-Delta function, and a is the diameter of the ring. If $z \gg r_0$ and $z \gg r_1$, from eqn (1) the lateral field distribution of the ring transducer can be derived:

$$\tilde{\Phi}(\tilde{r}_0, \omega) = \frac{2\pi a}{i\lambda z} e^{i\frac{2\pi}{\lambda}\left(z+\frac{a^2+r_0^2}{2z}\right)} J_0\left(\frac{2\pi a}{\lambda z} r_0\right), \tag{20}$$

where J_0 is the zeroth-order Bessel function of the first kind. The FWHM of the main lobe width of the zeroth-order Bessel function can be obtained from eqn (20):

$$\mathrm{FWHM}_R \approx 0.48 \frac{\lambda z}{a}. \tag{21}$$

Similar to eqns (5), (8), or (16), this equation demonstrates that for a given central wavelength, the FWHM of the beam produced by a ring transducer is a linear function of the ratio of the axial distance and the radius of the transducer.

Because the FWHM increases monotonically with z in eqn (21), the depth of field can also be defined as the distance between the two planes in which the FWHM increases or decreases to $\sqrt{2}$ times that at a reference axial distance. Therefore, the depth of field of the ring transducer is large and is given by eqn (18) with F replaced by z. However, energy efficiency of the ring transducer is rather low because only a small portion of the aperture is used (a thin ring). On the other hand, because the large depth of field of the ring transducer is formed at a large axial distance, the FWHM is also large (or the lateral resolution is low)

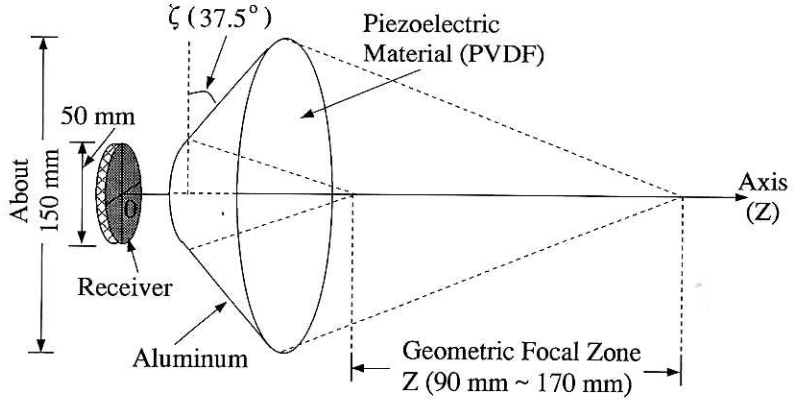

Fig. 6. Schematic of an Axicon transducer system evaluated by Fishell et al. (1990) in a clinic on female breasts. The cone has a large angle, $\zeta = 37.5°$, and thus has a high lateral resolution. It is used in transmission and has a large depth of field (focal zone: 90 ~ 170 mm). Because the cone has a huge diameter (about 150 mm), beams produced may be distorted severely in the breast tissues because of phase aberration. In reception, a smaller 5-element annular array transducer (50 mm diameter) is used to perform dynamic focusing (Foster et al. 1983).

except when the ring radius is large (eqn (21)). However, a large ring radius is not only inconvenient for medical diagnostic imaging, but could cause severe beam distortion due to tissue inhomogeneities (phase aberration) (Foster and Hunt 1979; Trahey et al. 1991). In addition, the sidelobes of the ring transducer (eqn (20)) are higher than those of the focused piston and Gaussian transducers (eqns (7) and (9)). The high sidelobes will lower contrast in medical imaging.

Axicon transducer. Another way to increase the depth of field is to use a conic device that is called the Axicon. The first Axicon was discovered in optics (McLeod 1954) and later applied to acoustics by Burckhardt et al. (1973b). Since then, the Axicon has been studied for medical imaging by many other investigators (Dietz 1982; Foster et al. 1981, 1983; Fujiwara 1962; Hunt et al. 1983; Moshfeghi 1988; Patterson and Foster 1982; Yamada and Shimizu 1983). A recent paper (Fishell et al. 1990) summarized the clinical trial of a "hybrid" Axicon system on patients with the hypothesis that the increased lateral resolution of a large Axicon transducer would lead to improved detection of smaller lesions and could thus contribute to the early detection of breast cancers. However, it turns out that the hypothesis is not true with the hybrid Axicon system after studying 1700 patients over 4 years. The system consisted of an Axicon of a maximum diameter of about 150 mm, an angle (Axicon angle is an angle between the cone and a transverse plane) of 37.5°, and focal zone from $z = 90 \sim 170$ mm (Fig. 6). The Axicon was made of a thin aluminum cone with the piezoelectric material (PVDF) attached to the inner surface of the cone (the PVDF was divided into eight sectors to perform signal processing for speckle reduction (Patterson et al. 1981; Kerr et al. 1986)). The FWHM of the Axicon beam was 0.3 mm and the central operating frequency was 4 MHz. In reception, a 5-element, 50 mm diameter dynamically focused annular array was used. This system was not operated in real time. One of the main reasons of the failure of the clinical application of the system might be the use of such a large diameter Axicon that has caused a severe distortion of the Axicon beam (phase aberration) in strongly inhomogeneous breast tissues (Foster and Hunt 1979; Trahey et al. 1991).

With CW excitation, the lateral distribution of the field of an unweighted Axicon in the focal zone can be derived from eqn (1) (under some assumptions, Patterson and Foster 1982)

$$\tilde{\Phi}(\vec{r}_0, \omega) \propto 2\pi \sin\zeta \sqrt{\frac{\cos\zeta}{\lambda}} \sqrt{z} e^{-i\left(\frac{2\pi}{\lambda} z\cos\zeta - \frac{\pi}{4}\right)} \cdot J_0\left(\frac{2\pi}{\lambda} r_0 \sin\zeta\right), \quad (22)$$

where ζ is the Axicon angle. It is seen that for a given central wavelength, λ, the lateral beamwidth in the focal zone depends only on the Axicon angle that is a constant for a given Axicon transducer. Therefore, an Axicon with a large angle can have a very sharp focus and produce a depth-independent high lateral resolution in imaging over the focal zone. The depth of field (the focal zone) is large for Axicons and is related to the maximum diameter of the cone (Fig. 6).

Unlike a conventional focused beam where its field strength peaks around the focus, the field strength of an unweighted Axicon increases with the axial distance in the focal zone (proportional to $\sqrt{z}$). However, the increase of the field strength could be compensated by applying a weighting along its radius (Dietz 1982). Equation (22) implies that the sidelobes of an Axicon are determined by the J_0 Bessel function, and are the same as those of a ring transducer (eqns (20)).

It is interesting to note here that Axicons produce waves similar to X waves (Lu and Greenleaf 1992a), which are limited diffraction beams and will be discussed in the next section. An X wave consists of two cones of pressure connected at their peak that are formed electrically by driving different signals at different radial distances of a transducer. The driving signals are obtained from the theoretical pressure distribution of the X wave evaluated at the surface of the transducer ($z = 0$). The "focal zones" of X waves start from the apex of the cones (or the surface of the transducer). In practical applications, the X waves are produced with an annular array transducer with a small Axicon angle (a few degrees rather than around 40 degrees for an Axicon). Because an annular array is used, echoes from tissues can be received with the same array in either a limited diffraction or dynamic focusing mode. This enables the X waves to be used in real-time imaging (using a commercial mechanical wobbler) with large depth of field and reasonable sidelobes (Lu et al. 1993).

Axial resolution

Another important factor for controlling the quality of pulse-echo imaging is the axial resolution. In general, a shorter pulse length produces a better axial resolution. Short pulses contain multiple frequency components and can only be produced by broadband transducers. If a transducer can be modeled approximately as a mass suspended by a spring moving in a lightly damped medium, the −3 dB bandwidth of the transducer is given by J. Krautkramer and H. Krautkramer (1975)

$$BW = \frac{f_r}{Q}, \tag{23}$$

where f_r is the resonant frequency of the transducer and

$$Q = \frac{\Delta d_{f_r}}{\Delta d_{\text{stat}}} = \frac{\pi}{\ln \eta} \tag{24}$$

is called the quality factor, where Δd_{f_r} and Δd_{stat} are the amplitude (at f_r) and the static thickness change (at zero frequency), respectively, and η is a damping coefficient. The damping coefficient is determined by the decay of the amplitudes of the free oscillation of the transducer after a brief excitation, *i.e.*, $\eta = A_1/A_2$, where A_1 and A_2 are the amplitudes of the first and second cycle of the oscillation, respectively. In typical medical imaging where a transducer is sandwiched with a backing and a front matching material, the damping coefficient is also given by

$$\eta = \begin{cases} \dfrac{(Z_0 + Z_b)(Z_0 + Z_f)}{(Z_0 - Z_b)(Z_0 - Z_f)}, & \text{if } Z_0 > Z_b \,\&\, Z_f, \text{ or } Z_0 < Z_b \,\&\, Z_f \\ \dfrac{(Z_0 + Z_b)^2(Z_0 + Z_f)^2}{(Z_0 - Z_b)^2(Z_0 - Z_f)^2}, & \text{if } Z_b > Z_0 > Z_f, \text{ or } Z_b < Z_0 < Z_f \end{cases}, \tag{25}$$

where Z_0, Z_b and Z_f are the acoustic characteristic impedances (density of a mass multiplied by speed of sound) of the transducer, backing and front matching materials, respectively (damping due to friction loss is not included). The resonant frequency of the transducer, f_r, is usually different from the characteristic frequency of the transducer

$$f_0 = \frac{c_0}{2d}, \tag{26}$$

where c_0 and d are the speed of sound and thickness of the transducer, respectively. However, if η is not too large, f_r and f_0 are close. In the second case of eqn (25), the characteristic frequency of the transducer is reduced by half from that given by eqn (26).

Equations (23), (24) and (25) demonstrate that the bandwidth can be increased by matching the characteristic impedances of both backing and front materials to that of the transducer (increases η). In medical imaging, the impedance of the transducer (such as lead zirconate-titanate (PZT)) is very different from that of biological soft tissues. In this case, the bandwidth can be increased directly by matching the impedance of the backing material to that of the transducer. However, this increases the loss of energy from the transducer into the backing material. Thus, in general, the increase of bandwidth will be at the expense of the transducer sensitivity or energy efficiency.

On the other hand, the useful energy of the transducer is the part that enters the biological soft tissues. To couple more energy into the tissues and further increase the bandwidth, one can add matching layers between the transducer and the tissues. These layers

will change the effective impedance of the tissues and improve the impedance matching. Another way to increase the bandwidth is to use multiple electrical excitations (Krautkramer and Krautkramer 1975; Lu et al. 1990). This method stops the transducer ringing by adding more electrical signals of proper amplitudes and phases. A method for two- and three-dimensional displays of acoustic pulses produced in water can be used to study transducers of different bandwidths (Lu et al. 1989).

LIMITED DIFFRACTION BEAM FORMING

Limited diffraction beams are a special class of solutions to the isotropic/homogeneous scalar wave equation. These solutions represent waves that would propagate to infinite distance without spreading, provided that they were produced with an infinite aperture and energy. By limited diffraction we mean that travelling with a wave in its propagation direction, one sees no changes in the wave pattern. Even if they are produced with a finite aperture and energy, the limited diffraction beams have a large depth of field and an approximate depth-independent property, *i.e.,* they have approximately unchanged beam shapes over a large axial distance. In this section, we review some of the limited diffraction beams and their potential applications.

Background

Beams with a large depth of field were first developed by Brittingham in 1983 (Brittingham 1983). He discovered electromagnetic waves that are localized solutions to the free-space Maxwell's equations and would propagate to an infinite distance with only local deformations. These waves were termed Focus Wave Modes (FWM). Based on Brittingham's work, two years later, Ziolkowski (Ziolkowski 1985) developed another wave that is also a localized solution to the isotropic/homogeneous scalar wave equation. This localized wave is a special case of Brittingham's FWM (eqns (46) and (47)) and was used to construct other localized waves such as modified-power-spectrum (MPS) pulses (Ziolkowski et al. 1989). Independent of Brittingham and Ziolkowski's work, Durnin discovered the first limited diffraction beams in 1987 in optics and called them nondiffracting or diffraction-free beams (Durnin 1987). To avoid the controversy of Durnin's terminologies, we have used the term "limited diffraction beams" (Lu and Greenleaf 1993b). Durnin's beams are also called Bessel beams because their lateral profile is a Bessel function. The property of the Bessel beams is that they would propagate to infinite distance without spreading provided that they were produced with an infinite aperture. Even if produced with a finite aperture, they are pencil-like and can focus over a large depth of field (Durnin et al. 1987).

Durnin's beams have been further studied in both optics (Cai et al. 1988; Gori et al. 1987a, 1987b; Indebetow 1989; Kielczynski and Pajewski 1991; Uehara and Kikuchi 1989; Vasara et al. 1989; Vicari 1989; Zahid and Zubairy 1989) and acoustics (Campbell and Soloway 1990). A narrow-band Bessel beam has been produced with an ultrasound transducer of a finite aperture using a nonuniform poling technique (Hsu et al. 1989). Broadband Bessel beams have been produced in water with an annular array transducer and applied to medical imaging (Lu and Greenleaf 1990b, 1991a, 1991c, 1991d, 1992f). Recently, a new class of nondispersive limited diffraction beams was discovered (Lu and Greenleaf 1991b, 1992a, 1992b, 1993d). These beams would not change their pulse shapes as they propagate to an infinite distance provided that they were produced with an infinite aperture and energy. Produced with a finite aperture and energy, these beams will have an approximately depth-independent point spread function over a large depth of field (Lu and Greenleaf 1992c, 1993a; Fatemi and Arad 1991, 1992; Fatemi and Ahanessians 1991). The nonspreading and nondispersive features of these beams may simplify the restoration of images (Lu and Greenleaf 1992c, 1992e). In addition, steering limited diffraction beams with a two-dimensional array transducer has also been studied (Lu and Greenleaf 1992d).

Theory

We begin by deriving a family of exact solutions to the scalar wave equation. In particular, the n-dimensional scalar wave equation for source-free, loss-less and isotropic/homogeneous media is given by (John 1982)

$$\left[\sum_{j=1}^{n} \frac{\partial^2}{\partial x_j^2} - \frac{1}{c^2}\frac{\partial^2}{\partial t^2}\right]\Phi = 0, \tag{27}$$

where x_j, $(j = 1, 2, \ldots, n)$, represent rectangular coordinates in an n-dimensional space, t is time, $n = 0, 1, 2, \ldots$, c is a constant representing the speed of wave and $\Phi = \Phi(x_1, x_2, \ldots, x_n; t)$ is an n-dimensional complex wave field. In the physical world, only the real or imaginary part of a complex wave is produced.

The wave eqn (27) has numerous solutions. One

family of solutions is given by Lu and Greenleaf (1992c):

$$\Phi(x_1, x_2, \ldots, x_n; t) = f(s), \tag{28}$$

where $f(s)$ is any well-behaved complex function of s, and

$$s = \sum_{j=1}^{n-1} D_j x_j + D_n(x_n - c_1 t), \tag{29}$$

in which

$$c_1 = \pm c\sqrt{1 + \sum_{j=1}^{n-1} D_j^2/D_n^2}, \tag{30}$$

where D_j are any complex coefficients, and $n \neq 0$ (otherwise $f(s)$ is only a function of time and represents a vibration). If D_j are properly chosen so that c_1 in eqn (30) is real, $f(s)$ represents a limited diffraction wave propagating along axis, x_n, at the phase velocity, c_1, in an n-dimensional space.

Infinite aperture Bessel beams and X waves

Limited diffraction beams such as Durnin's Bessel beams and the newly discovered X waves can be obtained from eqn (28) by properly choosing D_j and integrating eqn (28) over selected free parameters associated with D_j ($n = 3$) (Lu and Greenleaf 1992a):

$$\Phi_{J_m}(\vec{r}, t) = J_m(\alpha r)e^{i(\beta z - \omega t + m\phi)}, \tag{31}$$

and

$$\Phi_{X_m}(\vec{r}, t) = e^{im\phi}\int_0^\infty B(k)J_m(kr \sin \zeta)e^{-k[a_0 - i(z\cos\zeta - ct)]}dk, \tag{32}$$

where Φ_{J_m} and Φ_{X_m} are the m^{th}-order Bessel beams and X waves, respectively, $m = 0, 1, 2, \ldots$, J_m is the m^{th}-order Bessel function of the first kind, α is the scaling factor for the Bessel beams, $\beta = \sqrt{k^2 - \alpha^2} > 0$ (a condition that the Bessel beams exist) is a propagation constant, $r = \sqrt{x^2 + y^2}$ is a radial distance, $\phi = \tan^{-1}(y/x)$ is a polar angle, $\vec{r} = (r, \phi, z)$ is a spatial point in cylindrical coordinates, $k = \omega/c$ is a wave number, $B(k)$ represents any transmission or reception transfer function of a transducer (or antenna), ζ is an Axicon angle and a_0 is a constant that determines the decay rate of the high frequency components of the X waves.

The Bessel beams and X waves given by eqns (31) and (32) are limited diffraction solutions of the wave equation. It implies that these beams have infinite depth of field for any choices of the free parameters: α, ω, ζ and a_0. This is different from conventional beams. For example, the depth of field of a focused beam ($F < \infty$) is always finite, and the depth of field of an unfocused ($F = \infty$ in eqn (9)) Gaussian beam is also finite unless the central wavelength is zero. For the unfocused Gaussian beam, this is because its effective aperture size, σ, is finite. If $\sigma = \infty$, the unfocused Gaussian beam is actually a plane wave, which is a special case of the Bessel beam (with $\alpha = 0$ in eqn (31)) or X wave (with $\zeta = 0$ in eqn (32)) (the plane wave is also a limited diffraction beam).

At any given axial distance, say $z = 0$, the phase term in eqns (31) and (32) is $e^{-i(\omega t - m\phi)}$. This means that each frequency component of the wave rotates at a speed of ω/m (for $m \neq 0$) on the surface of the radiator. Therefore, they are also called waves of progressive phase (Burckhardt et al. 1973a) or rotating waves (Lu and Greenleaf 1993b).

For pulse-echo imaging applications, broadband beams are desirable. The broadband Bessel beams can be obtained by weighting eqn (31) with a transmitting transfer function, $T(\omega)$, and then linearly superposing the result over the angular frequency, ω (assume that the transducer is excited with an electrical δ-pulse)

$$\Phi_{JBB_m}(\vec{r}, t) = 2\pi e^{im\phi}J_m(\alpha r)\mathcal{F}^{-1}[T(\omega)e^{i\beta z}], \tag{33}$$

where the subscript "BB" means broadband, $\mathcal{F}^{-1}$ stands for the inverse Fourier transform that is defined as (Bracewell 1965)

$$g(t) = \mathcal{F}^{-1}\{G(\omega)\} = \frac{1}{2\pi}\int_{-\infty}^{\infty} d\omega G(\omega)e^{-i\omega t}, \tag{34}$$

and where $g(t)$ and $G(\omega)$ are a Fourier transform pair. Note that the broadband Bessel beams have also a depth-independent lateral beam profile (a depth-independent lateral resolution in imaging). However, the pulse shapes of the broadband Bessel beams vary with the axial distance, z, because the broadband Bessel beams are dispersive, *i.e.*, each frequency component of the beam travels at a different phase velocity.

From eqn (32), we obtain the m^{th}-order Broadband X wave if $B(k) = a_0$ (Lu and Greenleaf 1992a)

$$\Phi_{XBB_m} = \frac{a_0(r \sin \zeta)^m e^{im\phi}}{\sqrt{M}(\tau + \sqrt{M})^m}, \tag{35}$$

where $M = (r \sin \zeta)^2 + \tau^2$, in which $\tau = [a_0 -$

$i(z \cos \zeta - ct)$]. Because $B(k)$ in eqn (32) is arbitrary, it can be used to represent a transmitting transfer function of a practical transducer. Because the transfer functions of practical transducers are usually band-limited, the X waves produced by these transducers are given by

$$\Phi_{XBL_m} = \frac{1}{a_0} \mathcal{F}^{-1}\left[B\left(\frac{\omega}{c}\right)\right] * \Phi_{XBB_m}, \tag{36}$$

where the subscript "BL" means band-limited and "$*$" represents convolution in terms of time. Because each frequency component travels at a constant speed, $c_1 = c/\cos \zeta$, the X waves in eqns (35) and (36) are nondispersive.

The X waves given by eqn (32) or (36) include some specific X waves studied recently. Although these specific X waves have different field distributions around their wave centers as compared to the broad-band X waves given by eqn (35), they all possess a similar asymptotic behavior in their sidelobes (X branches). Letting $B(k) = -i\omega a_0$, we have the first derivative of the X waves in eqn (35)

$$\frac{\partial \Phi_{XBB_m}}{\partial t} = -ica_0(r \sin \zeta)^m e^{im\phi} \cdot \frac{[\tau(\tau + (m+1)\sqrt{M}) + mM]}{(\sqrt{M})^3(\tau + \sqrt{M})^{m+1}}. \tag{37}$$

If $m = 0$ and multiplying eqn (37) by a constant, $-\cos^2\zeta/(ica_0)$, one obtains the X wave described by Donnelly et al. (1994) by assuming $\gamma z_0 = a_0$ and $\gamma = \cos \zeta$ in their notations.

Another special X wave can be derived by letting $B(k) = -\omega^2 a_0$, which is a second derivative of eqn (35)

$$\frac{\partial^2 \Phi_{XBB_m}}{\partial t^2} = c^2 a_0(r \sin \zeta)^m e^{im\phi} \cdot \left\{\frac{M[(1-2m)\tau + (1-m^2)\sqrt{M}]}{(\sqrt{M})^5(\tau + \sqrt{M})^{m+1}} - \frac{3\tau^2[\tau + (m+1)\sqrt{M}]}{(\sqrt{M})^5(\tau + \sqrt{M})^{m+1}}\right\}. \tag{38}$$

For $m = 0$, eqn (38) gives the X wave that is derived by Zou et al. (1993) using the wavelet transform (dividing by the constant $-c^2 a_0$).

For one-dimensional linear array applications, unsymmetrical limited diffraction beams that are also solutions of the wave eqn (27) are desirable. Because the order of derivatives is exchangeable, any partial-derivatives of a solution of eqn (27) with respect to the variable, x_j or t, and their linear combinations are still solutions. Unsymmetrical X waves can be constructed from eqn (35), for example

$$a_1 \frac{\partial^2 \Phi_{XBB_0}}{\partial x^2} + a_2 \frac{\partial^2 \Phi_{XBB_0}}{\partial y^2} = a_0 \sin^2\zeta \cdot \left\{\frac{[(2a_1 - a_2)x^2 + (2a_2 - a_1)y^2]\sin^2\zeta}{(\sqrt{M})^5} - \frac{(a_1 + a_2)\tau^2}{(\sqrt{M})^5}\right\}, \tag{39}$$

where $m = 0$, and a_1 and a_2 are constants. If $2a_1 - a_2 > 0$ and $2a_2 - a_1 > 0$ simultaneously, the numerator of eqn (39) in a transverse plane ($x - y$ plane) represents elliptic contours with two axes proportional to $\sqrt{2a_2 - a_1}$ and $\sqrt{2a_1 - a_2}$, respectively. The above equation could also be used to simplify the electronic steering of limited diffraction beams with a two-dimensional array (Lu and Greenleaf 1992d).

Finite aperture Bessel beams and X waves

In practical applications of limited diffraction beams, the apertures of transducers used to produce the beams are finite. In this case, limited diffraction beams such as the Bessel beams and X waves have a finite depth of field and can be approximately produced by truncating the infinite aperture beams given by eqns (33) and (35) at the transducer surfaces ($z = 0$). Broad-band pulses for $z > 0$ can be obtained by first calculating the fields for all frequencies with eqn (1), with the aperture weighting function, $\tilde{\Phi}(\vec{r}_1, \omega)$, obtained from the temporal Fourier transform of eqn (33) or (35), and then doing the inverse Fourier transform of the results with eqn (34).

If an aperture is circular and its radius is a, the depth of field of the Bessel beams and X waves produced by the aperture is given by (Durnin 1987; Lu and Greenleaf 1992a)

$$BZ_{\max} = a\sqrt{(k/\alpha)^2 - 1}, \tag{40}$$

and

$$XZ_{\max} = a \cot \zeta, \tag{41}$$

respectively. The depth of field here is defined as the

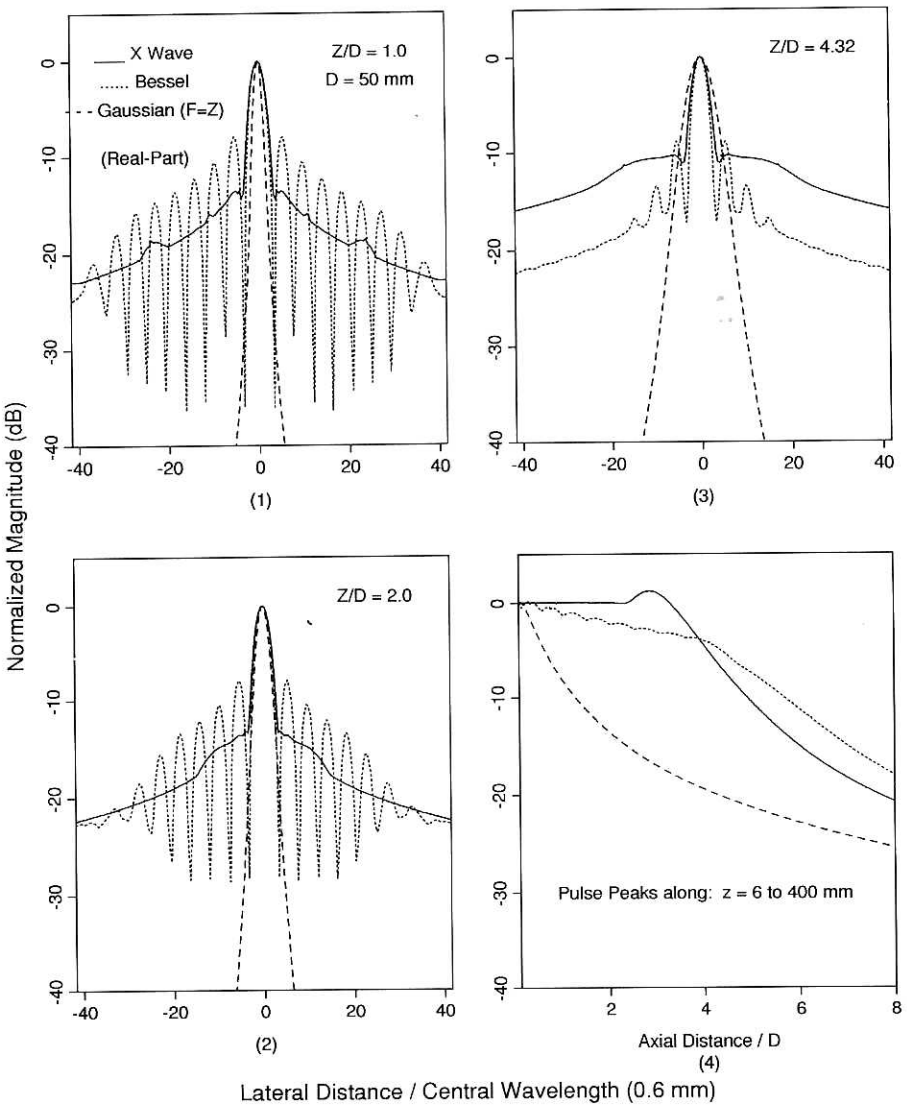

Fig. 7. Sidelobes and depth of field of a zero[th]-order X wave (full lines), J_0 Bessel beam (dotted lines) and dynamically focused ($F \equiv Z$) Gaussian beam (dashed lines) produced with an aperture of diameter of 50 mm at a central wavelength of 0.6 mm (2.5 MHz central frequency). Real part of complex beams are plotted. The lateral plots of the beams are given at three depths: (1) 50, (2) 100 and (3) 216 mm. The peaks of pulses are plotted as the beams propagate from 6 to 400 mm (4).

distance in which the field maximum drops to about one half of that at the surface of the transducer. For both the Bessel beams and X waves, the depth of field increases linearly with the size of aperture.

Examples of a J_0 Bessel beam and a zero[th]-order X wave ($m = 0$) calculated from eqn (1) are shown in Fig. 7 (with exact aperture weightings). The lateral plots of the beams show the sidelobes where the maxima of the field along lines parallel to the wave axis are plotted vs. the lateral distance. For the Bessel beam, the scaling factor, $\alpha = 1202.45\ \mathrm{m}^{-1}$, and the transmitting transfer function, $T(\omega)$, is the Blackman window function (Oppenheim and Schafer 1975) that is peaked at the central frequency $f_0 = 2.5$ MHz with a relative bandwidth of about 81% (−6 dB bandwidth divided by the central frequency). For the X wave, $a_0 = 0.1$ mm, $\zeta = 6.6°$ and the transmitting transfer function, $B(k)$, is the same as $T(\omega)$. The radius of the aperture, a, is 25 mm and the speed of sound, c, is 1500 m/s. The depth of field calculated from eqns (40) and (41) for the Bessel beam and X wave are about 216.3 mm and 216.1 mm, respectively. For comparison, a dynamically focused Gaussian beam is also shown. The FWHM of the Gaussian beam at the transducer surface

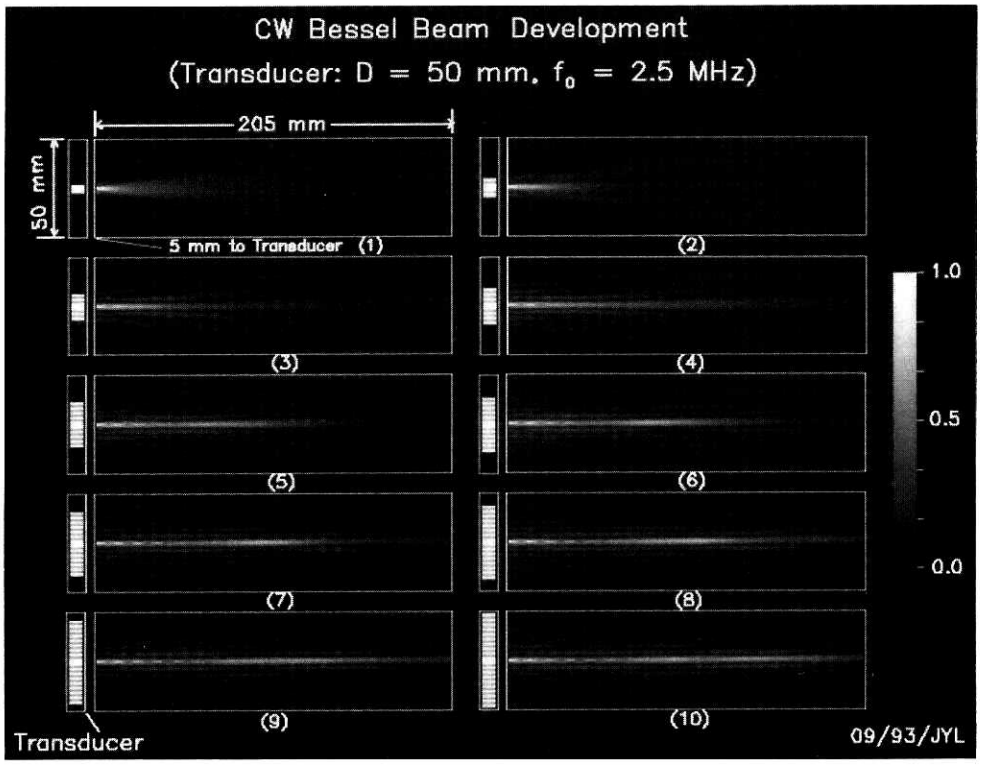

Fig. 8. Development of a CW J_0 Bessel beam (sagittal cross-section) measured in water as more of the aperture (indicated with white bars on the left hand side of each panel) of an annular array transducer is excited. The array has 10 elements and a diameter of 50 mm. It is weighted with a stepwise Bessel function. The frequency of the beam is 2.5 MHz and the scaling parameter, α, is 1202.45 m^{-1}. The depth of the beam is about 216.28 mm. Panels (1) to (10) correspond to one to ten elements excited, respectively. Modified with permission from Fig. 2 of Lu and Greenleaf 1993d.

is 25 mm (or σ = 15.014 mm). The focal length of the beam is equal to the observation distance, *i.e.*, $F \equiv z$. The transmitting transfer function of the transducer is the same as that for the Bessel beam.

The weighting function, $\tilde{\Phi}(\tilde{r}_1, \omega)$, in eqn (1) can be approximated with stepwise functions such as one determined by a 10-element annular array transducer (Lu and Greenleaf 1991a, 1992b). The use of an annular array transducer to produce limited diffraction beams will simplify the construction of the transducer and allow the currently available annular array technology to be used. Moreover, it is convenient to use the same annular array transducer to produce either a limited diffraction beam or a conventional beam, or to perform dynamically focused reception in pulse-echo imaging to suppress the high sidelobes of limited diffraction beams in transmission (Lu et al. 1993). Figures 8, 9 and 10 show the CW J_0 Bessel beam, J_0 Bessel pulse and zeroth-order X waves and how they develop in water as more active rings of the 10-element annular array transducer are excited (Lu and Greenleaf 1993d).

Trade-off between lateral resolution and depth of field

With a finite aperture, there is a trade-off between the depth of field and the FWHM (lateral resolution of images) of limited diffraction beams. The FWHM of the broadband Bessel beams and X waves can be obtained from eqns (33) and (35) with $m = 0$ (the beams have a central maximum), respectively (Lu and Greenleaf 1992a)

$$\text{FWHM}_B \approx \frac{3.04}{\alpha}, \tag{42}$$

and

$$\text{FWHM}_X \approx \frac{2\sqrt{3}a_0}{\sin \zeta}, \tag{43}$$

where the subscripts "B" and "X" represent the Bessel beams and X waves. The FWHM is calculated in the transverse planes through the pulse centers. To

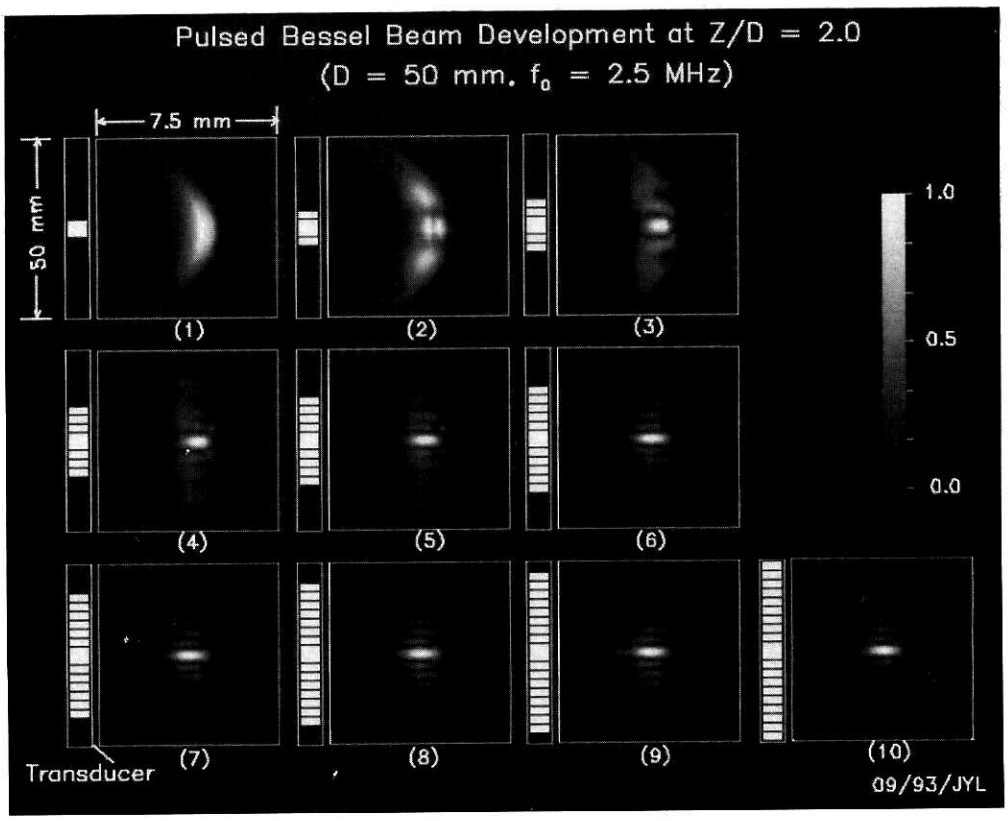

Fig. 9. Development of a J_0 Bessel pulse (sagittal cross-section) measured in water at $Z/D = 2.0$ (where Z and D are axial distance and transducer diameter, respectively) as more of the aperture (indicated with white bars on the left hand side of each panel) of an annular array transducer is excited. The same transducer array in Fig. 8 is used and its weighting is also the same, but the transducer is driven with a one-and-a-half cycle pulse. Modified with permission from Fig. 3 of Lu and Greenleaf 1993d.

increase the lateral resolution, the free parameters α and ζ in eqns (42) and (43) must also be increased. This is in conflict with the depth of field given by eqns (40) and (41).

On the other hand, the depth of field and the FWHM are related directly or indirectly to the central frequency (central wavelength) of the beams. Although a higher central frequency does not increase directly the lateral resolution of the Bessel beams (eqn (42)), it increases the depth of field (eqn (40)). To keep the same depth of field (eqn (40)), α should be increased. This increases the lateral resolution (eqn (42)). Similarly, a smaller a_0 in eqn (43) increases the high frequency components of X waves (eqn (32)) and increases the lateral resolution directly while keeping the same depth of field (eqn (41)). The trade-off between the depth of field and the lateral resolution of limited diffraction beams, and its dependence on the central frequency (or wavelength), are similar to those of conventional beams (eqns (15) and (16)).

A method to increase both the lateral resolution and the depth of field of X waves has been developed recently (Song et al. 1993). In the method, the Axicon angle, ζ, is modified as a function of radial distance, $\zeta(r_1) = \zeta_0 - \zeta_1\sqrt{r_1/a} > 0$, at the surface of a transducer, where ζ_0 and ζ_1 are constants. This increases the lateral resolution of the X waves at distances closer to the transducer, while keeping a larger depth of field (eqns (41) and (43)) because the Axicon angle decreases as the radial distance increases (Lu and Greenleaf 1992a). However, the modified X waves are no longer limited diffraction solutions to the wave eqn (27) even if they were produced with an infinite aperture.

Sidelobe reduction

The sidelobes of the Bessel beams and X waves are at about the same level as those of a Bessel function (eqns. (31), (32) and (33)) and thus are very high. High sidelobes reduce contrast in imaging, making early detection of small cysts and tumors difficult. In addition, high sidelobes lower the accuracy in tissue character-

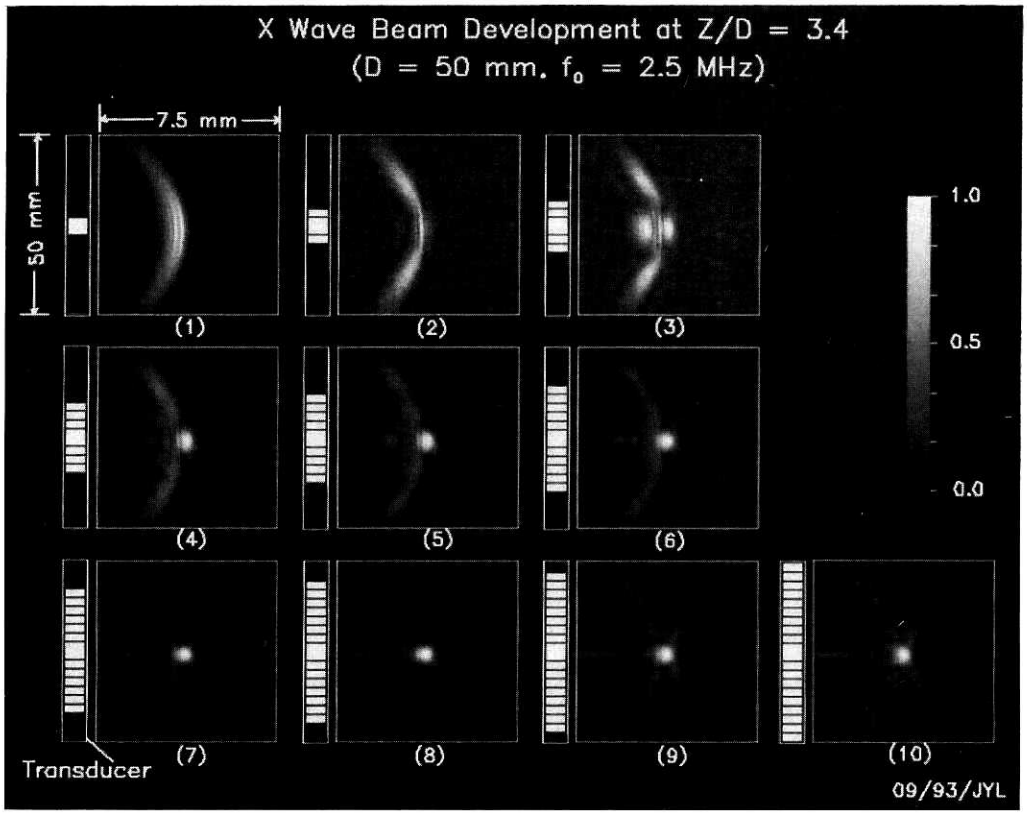

Fig. 10. The same format as that in Fig. 8, except that a zero[th]-order X wave measured in water at $Z/D = 3.4$ is displayed. The X wave has the following parameters: $a_0 = 0.05$ mm, $\zeta = 4.0°$ and a depth of field of 357.51 mm. The transducer is the same as that used in Fig. 9 but weighted with eqn (35) with both z and $n = 0$. Modified with permission from Fig. 6 of Lu and Greenleaf 1993d.

ization (identification) and increase background noise in nondestructive evaluation of materials.

Summation-subtraction method. A method to reduce the sidelobes of limited diffraction pulse-echo imaging systems in which limited diffraction beams are used in both transmission and reception has recently been developed (Lu and Greenleaf 1993b). To implement the method, nonrotating limited diffraction beams are developed as follows

$$\Phi'_{J_m}(\vec{r}, t) = J_m(\alpha r)\cos m(\phi - \phi_0)e^{i(\beta z - \omega t)}, \quad (44)$$

and

$$\Phi'_{X_m}(\vec{r}, t) = \cos m(\phi - \phi_0) \cdot \int_0^\infty B(k)J_m(kr \sin \zeta)e^{-k[a_0 - i(z\cos\zeta - ct)]}dk, \quad (45)$$

where ϕ_0 is an initial rotation angle of the beams. Note that eqns (44) and (45) are the same as eqns (31) and (32), respectively, except that $e^{im\phi}$ is replaced with $\cos m(\phi - \phi_0)$. The prime is used to distinguish eqns (44) and (45) from eqns (31) and (32), respectively.

Sidelobes of the pulse-echo imaging systems using the limited diffraction beams in eqns (44) and (45) can be reduced by summing echoes produced from the second-order beams that are rotated around the beam axis by $\pi/4$ with each other, and then subtracting the result from the echoes obtained with the zero[th]-order beams. The reason that the sidelobes can be reduced is because $\cos^2 m\phi + \cos^2 m(\phi - \pi/(2m)) \equiv 1$ for any m, and $J_0^2(\cdot)$ and $J_2^2(\cdot)$ approach to the same function as their arguments increase. The square operation for both the cosine and Bessel function comes from the pulse-echo process. It is the square operation that cancels the azimuthal-angular dependence of the higher-order limited diffraction beams. A 25 mm diameter, 3.5 MHz central frequency and 14-element annular array transducer of 16 sectors has been suggested to implement the summation-subtraction sidelobe reduction (Lu and Greenleaf 1993c).

The sidelobe reduction method above requires

three A-lines that need three transmissions at one transducer position. This reduces frame rate to $\frac{1}{3}$ in imaging. More higher-order limited diffraction beams can be used to further reduce the sidelobes (Wild 1965). But this lowers further the imaging frame rate. The trade-off between sidelobes and imaging frame rate for limited diffraction beams is similar to that between depth of field and frame rate for conventional focused beams. Conventional beams have low sidelobes at their focuses. Their depth of field is usually increased with a montage process that lowers the imaging frame rate, but low frame rate produces artifacts for images of fast moving objects such as the heart.

Although the depth of field of conventional beams is increased after a montage process, they are still diffracting within their depth of field. This is seen from eqn (16) where the FWHM of a Gaussian beam at focus is a linear function of its focal length. In contrast, both the zero[th]- and higher-order limited diffraction beams are nearly nonspreading within their depth of field. Consequently, after sidelobe reduction, they are still nonspreading. This may simplify image restorations such as deconvolution for limited diffraction imaging systems because the point spread functions of the systems are approximately depth-independent or shift-invariant. In addition, the FWHM of limited diffraction beams will not change with the speed of sound of materials imaged, although their depth of field may be reduced at a higher speed of sound (larger central wavelength). This is convenient in nondestructive evaluation of materials where the speed of sound of materials could vary significantly from one application to another (Lu and Greenleaf 1993a).

Deconvolution. Because the point spread functions of limited diffraction pulse-echo imaging systems are approximately depth-independent, image restoration techniques such as deconvolution are readily applied to reduce the sidelobes. An example was given to restore an image obtained with a J_0 Bessel beam using a Wiener filtering technique. The result showed that with only one filtering kernel, the sidelobes were reduced around 10 dB over the entire depth of interest, in addition to an enhancement of both lateral and axial resolutions (Lu and Greenleaf 1992c, 1992e).

Limited diffraction transmission and dynamically focused reception. A pulse-echo imaging system may take the advantages of both limited diffraction beams and conventional beams if limited diffraction beams are used in transmission and conventional beams in dynamically focused reception. Such "hybrid" systems may produce high frame rate, large depth of field and low sidelobe images (Lu et al. 1993) because the high sidelobes of limited diffraction beams are suppressed by the low sidelobe dynamically focused reception. In addition, if dynamic focused reception with a constant f-number is used (eqn (8)), such "hybrid" imaging system can be expected to have an approximate depth-independent point spread function and thus various image restoration techniques can be readily used to improve image quality.

Localized waves. Localized waves were first discovered by Brittingham and were termed Focus Wave Modes (FWM) (Brittingham 1983). These waves contain phase terms that represent waves propagating at two different speeds. The FWM discovered by Brittingham are the linear combinations of the terms of the form

$$\Phi^m_{\mathrm{FWM}_B}(\vec{r}, t) \propto \frac{r^{m_1} e^{-\frac{k_1 r^2}{[z_0 + i(z-ct)]} \cdot \frac{c-c_1}{c+c_1}}}{[z_0 + i(z - ct)]^{m_2}} e^{-ik_1(z-ct)} e^{ik_2(z-c_1 t)} \begin{Bmatrix} \sin m\phi \\ \cos m\phi \end{Bmatrix}, \quad (46)$$

where z_0 is a real constant, m, m_1 and m_2 are integers that are interrelated, $c > c_1 > 0$, k_1 is a positive real constant and $k_2 = 2ck_1/(c + c_1)$. Equation (46) includes another FWM that was derived two years later by Ziolkowski (1985) using a complex source location approach. Letting m, $m_1 = 0$, $m_2 = 1$ and $c_1 = 0$, and multiplying the constant $1/(4\pi i)$ in eqn (46), we have (Ziolkowski 1985)

$$\Phi_{\mathrm{FWM}_Z}(\vec{r}, t) = \frac{e^{-\frac{k_1 r^2}{[z_0 + i(z-ct)]}}}{4\pi i[z_0 + i(z - ct)]} e^{ik_1(z+ct)}. \quad (47)$$

A linear summation over the free parameter, k_1, produces the so-called modified-power-spectrum (MPS) pulse that has a finite total energy (Ziolkowski et al. 1989)

$$\Phi_{\mathrm{MPS}}(\vec{r}, t) = R_e \left\{ \frac{e^{-b_1\left(\frac{r^2}{[z_0 + i(z-ct)]} - i(z+ct)\right)/b_2}}{[z_0 + i(z - ct)] \cdot \left(\frac{r^2/[z_0 + i(z + ct)] - i(z + ct)}{b_2} + b_3\right)^{b_4}} \right\}, \quad (48)$$

where "R_e" represents the real part; b_1, b_2, b_3 and b_4 are constants. Because there are terms $z - ct$ and $z - c_1 t$, or $z - ct$ and $z + ct$ in eqns (46), (47) and (48), the waves represented by these equations are not limited

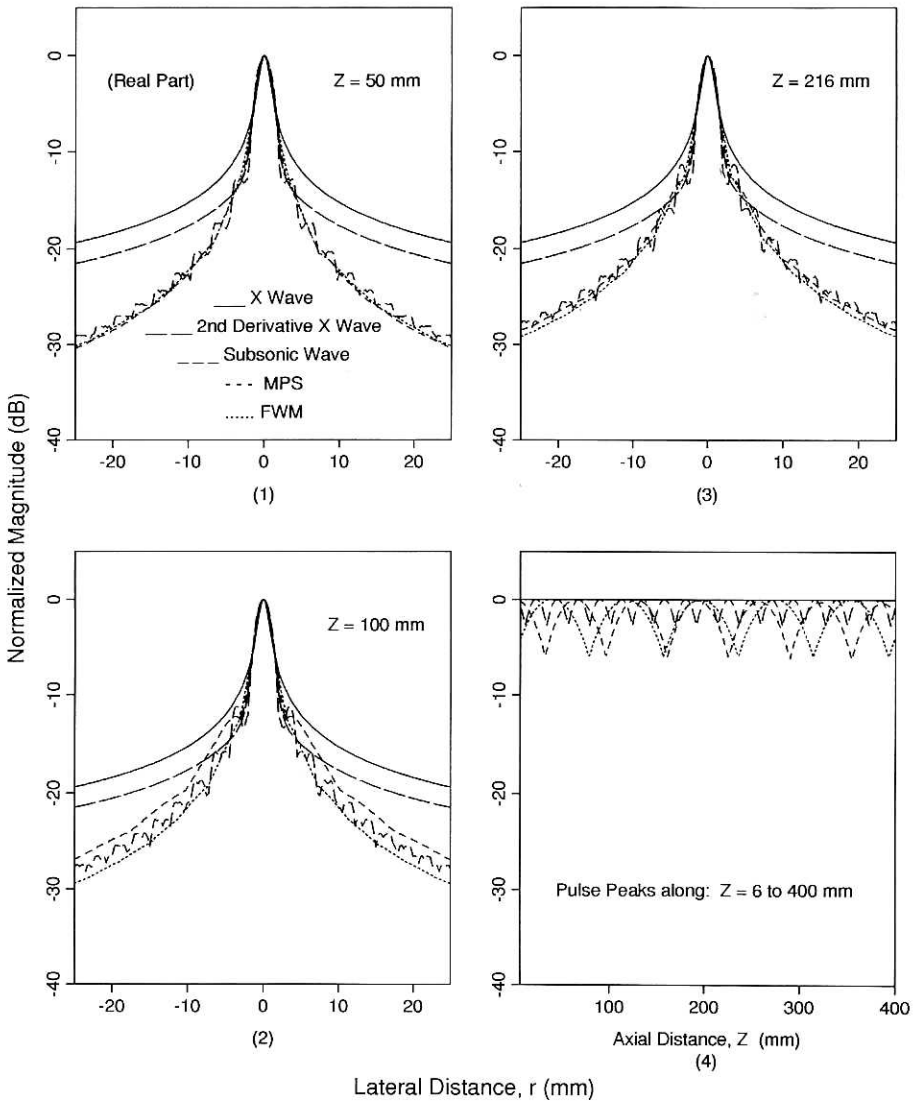

Fig. 11. Sidelobes and peaks of pulses of the special class of solutions of the scalar wave equation for zeroth-order X wave (Full lines), zeroth-order second-derivative X wave (very long dashed lines), subsonic (subluminal) wave (long dashed lines), modified-power-spectrum (MPS) pulse (dashed lines) and focus wave mode pulse (FWM) (dotted lines). The sidelobes are plotted at three depths: (1) 50, (2) 100 and (3) 216 mm. The peaks of pulses along the propagation axis are plotted (Panel 4) to show the fluctuations of the beams and their infinite depth of field when they are produced with an infinite aperture, except MPS whose depth of field is finite because it has a finite total energy (the amplitude of its peaks has already dropped slightly within the relatively small propagation depth of 400 mm).

diffraction beams. The real and imaginary part of these waves are functions of the axial distance, z, even if one travels with the waves ($z = ct$). However, these waves can be localized around the wave center by properly choosing their free parameters.

The sidelobes of localized waves are lower than those of X waves. A lateral plot of eqns (47) and (48) is shown in Fig. 11 (compared with the X wave (eqn (35)) and second-derivative X wave (eqn (38)) of m = 0). The maxima of the beams along lines parallel to the wave axis are plotted versus the radial distance to show the sidelobes. However, when the localized waves in Fig. 11 are produced by a band-pass linear transducer system whose transmitting transfer function is a Blackman window function similar to that of physical ultrasound transducers in medical imaging, their sidelobes are about the same as those of the X waves (Fig. 12). In other words, if the transducer system had

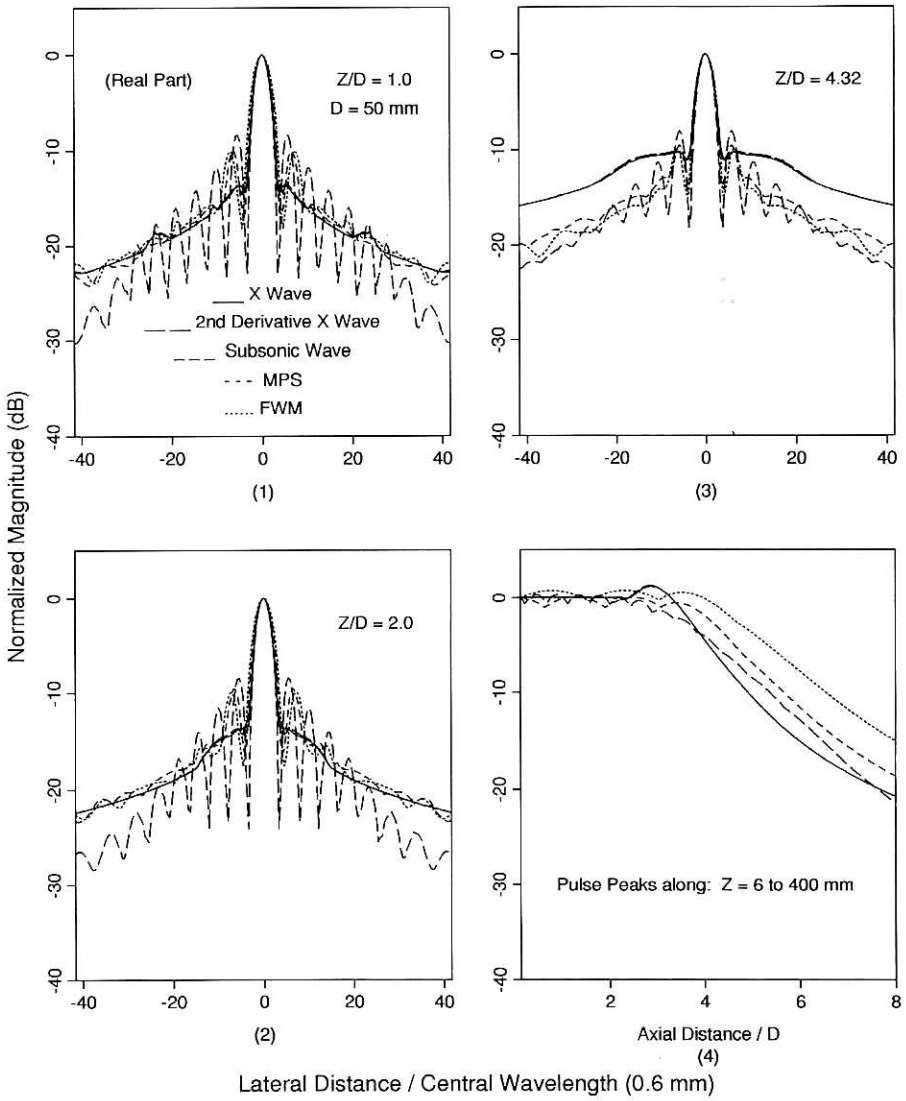

Fig. 12. Beams produced with a finite aperture and band-limited transducer. They correspond to the beams in Fig. 11. The figure has the same format as Fig. 7.

a flat frequency response (infinite bandwidth), the sidelobes of the localized waves would be lower. This means that the localized waves contain more high frequency components than the X waves. The fourth panel of Fig. 11 shows the fluctuations of the pulse peaks (on or around the pulse centers) of the localized waves as they propagate. The fluctuations are reduced as the waves are band-pass filtered (Panel 4 of Fig. 12). The radius of the aperture for producing the beams in Fig. 12 is the same as that for those in Fig. 7 (25 mm).

The FWHM of the beams in Fig. 11 is adjusted to about the same as that of the X waves with the parameters of the beams chosen as follows: for the X wave, $a_0 = 0.1$ mm, $\zeta = 6.6°$; for the second-derivative X wave, $a_0 = 0.35$ mm, $\zeta = 6.6°$; for the FWM in eqn (47), $z_0 = 6.0 \times 10^{-5}$ m, $k_1 = 20.0$ m^{-1}; and for the MPS in eqn (48), $z_0 = 6.0 \times 10^{-5}$ m, $b_1 = 60.0$ m^{-1}, $b_2 = 2.5$, $b_3 = 1.0$ m, $b_4 = 1.0$. The speed of sound, c, is assumed to be 1500 m/s.

After filtering with the Blackman window function (the same as that for Fig. 7), the FWHM of the localized waves is slightly increased from that of the X waves, and thus the -6 dB depth of field of beams is also increased (Panel 4 in Fig. 12). In addition, the second-derivative X wave is almost the same as the X wave after the filtering (their curves almost overlap in Fig. 12). The other parameters of the beams in Fig. 12 are the same as those in Fig. 11.

Subsonic (subluminal) waves. X waves and Bessel beams are also supersonic (superluminal (Donnelly and Ziolkowski 1993)) waves because their phase velocities are greater than the speed of sound or light, c (eqns (31) and (35)). Subsonic (subluminal (Donnelly and Ziolkowski 1993)) waves are waves whose peak propagates slower than c. A subsonic (subluminal) wave was derived recently with a method that solves the isotropic/homogeneous scalar wave equation in a temporal-spatial Fourier transform domain (Donnelly and Ziolkowski 1992, 1993)

$$\Phi_{\text{Sub}}(\vec{r}, t) = \frac{\sin\left[\frac{\xi}{\sin^2\zeta}\sqrt{(z - (c\cos\zeta)t)^2 + (r\sin\zeta)^2}\right]}{\frac{\xi}{\sin^2\zeta}\sqrt{(z - (c\cos\zeta)t)^2 + (r\sin\zeta)^2}} \cdot e^{i\frac{\xi\cos\zeta}{\sin^2\zeta}\left(z - \frac{c}{\cos\zeta}t\right)}, \quad (49)$$

where the subscript "Sub" means subsonic or subluminal, and ξ and ζ are constants. We have obtained the spectrum of $\Phi_{\text{Sub}}(\vec{r}, t)$ by looking up an integration table (Gradshteyn and Ryzhik 1980)

$$\tilde{\Phi}_{\text{Sub}}(\vec{r}, \omega) = \frac{\pi\sin^2\zeta}{\xi c\cos\zeta} e^{i\left(\frac{\omega}{c} - \xi\right)\frac{1}{\cos\zeta}z} \cdot J_0\left(r\tan\zeta\sqrt{\left(\frac{\xi\cos\zeta}{\sin^2\zeta}\right)^2 - \left|\frac{\omega}{c} - \frac{\xi}{\sin^2\zeta}\right|^2}\right), \quad (50)$$

where $0 < \left|\frac{\omega}{c} - \frac{\xi}{\sin^2\zeta}\right| < \frac{\xi\cos\zeta}{\sin^2\zeta}$. The subsonic wave in eqn (49) is also a localized wave. The peak of the real or imaginary part of the subsonic wave is also fluctuating as it propagates because a phase term of eqn (49) travels at a supersonic speed, $c/\cos\zeta$. A lateral plot of eqn (49) is also shown in Fig. 11. The subsonic localized wave is emphasized because its frequency components are in a finite range.

The field of the subsonic wave vs. the radial distance is a sinc function (eqn (49)). Thus, the sidelobes of the subsonic wave are lower than those of the Bessel beams (eqn (31)) or X waves (eqn (32)) whose dependence of fields on the radial distance is similar to that of a Bessel function (Fig. 11). The subsonic wave given by eqn (49) has a broad bandwidth. Its lowest and highest frequency components are given by $f_l = (1 - \cos\zeta)f_0$ and $f_h = (1 + \cos\zeta)f_0$, respectively, where $f_0 = \xi c/(2\pi\sin^2\zeta)$ is the center frequency. This means that if a transducer system has a flat frequency response over the above frequency range, the subsonic wave with lower sidelobes can be produced. With a finite aperture, the depth of field of the subsonic wave may be finite, but a broadband subsonic wave will retain its low sidelobes over a large depth of field (this can be verified by a simulation with eqn (1)).

If the transmitting transfer function of the transducer is a Blackman window function peaked at f_0, the sidelobes of the subsonic wave are increased greatly (Fig. 12) and are at about the level of the X waves. This is because the transducer system eliminates the high-frequency components of the wave. The high-frequency components decrease diffractive spreading, thus increasing depth of field and also lowering the sidelobes with the same depth of field.

The parameters for the subsonic waves in Figs. 11 and 12 are as follows: $\zeta = 6.6°$ and $\xi = 138.34$ m^{-1}. With the above parameters, the central frequency of the Blackman window function is about 2.5 MHz (the same as that for Fig. 7), and the lowest and highest frequencies of eqn (49) are 0.017 and 4.98 MHz, respectively. The relative bandwidth of the broadband subsonic wave is given by $2\cos\zeta = 199\%$. In practice, a transducer system that has such a huge relative bandwidth while still having high sensitivity would be difficult to obtain. The aperture radius for the simulation of the subsonic wave in Fig. 12 is the same as that for other beams (25 mm).

Possible applications

Because limited diffraction beams have very large depth of field and are approximately depth-independent even if they are produced with a finite aperture, they could have practical applications in enhancing the lateral resolution while keeping a high frame rate in medical imaging (Lu and Greenleaf 1990b), eliminating diffraction correction in tissue characterization (Lu and Greenleaf 1990a), having material-independent and depth-independent lateral resolution and simplifying image processing in nondestructive evaluation of materials (Lu and Greenleaf 1993a), Doppler imaging (Evans et al. 1989; Hein and O'Brien 1993; Magnin 1987), as well as other wave related areas such as energy transmission in electromagnetics (Brittingham 1983; Ziolkowski 1989) and laser energy transfer and optical alignment in optics (Ojeda-Castaneda and Noyola-Iglesias 1990). However, the sidelobes of limited diffraction beams are high and must be accounted for in imaging applications. As is seen from the last subsection, the reduction of sidelobes is usually at the

expense of imaging frame rate or the bandwidth of a transducer system.

BEAM STEERING

To form an image, sweeping a beam over a cross-section of an object is necessary. In medical imaging, two methods are used to sweep beams: mechanical and electronic. For each method, two scan formats are usually used: linear and sector.

Mechanical scan

In a mechanical scan, a beam is swept by moving or wobbling the transducer with a stepping motor to perform a linear or sector scan (Foster et al. 1989a, 1989b). The linear scan usually requires a larger acoustic window, while the sector scan uses a smaller one. Therefore, the sector scan is particularly useful in cardiac imaging where the window sizes are limited by surrounding bones. The mechanical scan does not need complex electronic circuitry. It maintains the same beam quality (sidelobes and beamwidth, etc.) over all transducer positions or angles if the refraction of beams on the interface between coupling fluid and the objects imaged is negligible (Foster et al. 1989a). However, the mechanical scan has the following limitations: (1) the frame rate is limited by the inertia of the transducer and the motor system; (2) it is difficult to maintain a constant speed in transducer wobbling; (3) the transducer may vibrate when it is operated; (4) the system is subject to mechanical wear and (5) the transducer is difficult to start and stop abruptly to shoot a beam several times in each transducer position, as is desired in conventional real-time color Doppler imaging (Evans et al. 1989; Magnin 1987).

Electronic scan

An electronic scan is usually produced with array transducers. There are two types of array transducers: one- and two-dimensional array transducers (Kino 1987). A one-dimensional array has its elements arranged in a line, while a two-dimensional array consists of elements that are arranged in a plane. In a linear scan, the elements of an array transducer are excited or multiplexed one by one or group by group sequentially in one direction to sweep a beam. In the sector scan, a beam is steered by signals that are applied to the elements of an array with delays that are a linear function of the element positions in the scan direction. An electronic sector scan with an array transducer may distort the beams, lowering the lateral resolution or destroying some beams, such as the limited diffraction beams (Lu and Greenleaf 1992d). This is because the effective size of the aperture of the transducer is reduced as the beam is steered off the normal axis of the transducer. In addition, the sidelobes and grating lobes of the beams may be increased in the sector scan because the element sizes are not small enough and the number of elements is not large enough.

One-dimensional array. One-dimensional arrays are widely used in modern commercial ultrasound scanners for medical diagnosis because they have a relatively few number of elements (von Ramm and Smith 1983). Beams can be focused dynamically by a one-dimensional array in a lateral plane or scan plane (determined by the line of array elements and the axial axis of the array). In the plane that is perpendicular to the scan plane (elevation plane), the beams can only be focused with an acoustic lens that has a fixed focal length. Therefore, the slice thickness of an image obtained by a one-dimensional array will be large and depth dependent. In addition, one-dimensional arrays cannot scan electronically in the elevation plane.

Two-dimensional array. Two-dimensional arrays contain a large number of elements (from a few hundreds to a few thousands) in order to reduce grating lobes. They are difficult to construct because their dimensions are usually of the order of a few centimeters (in medical imaging). Most current studies of two-dimensional arrays are theoretical and computer simulations (Turnbull and Foster 1991, 1992a), although some prototypes of two-dimensional arrays have been constructed (Turnbull and Foster 1992b; Smith et al. 1991). Nevertheless, two-dimensional arrays are promising for volumetric (three-dimensional) imaging, phase-aberration correction, slice thickness reduction, and steering of limited diffraction beams (Smith et al. 1991; Nock and Trahey 1992; Lu and Greenleaf 1992d). Practical applications of two-dimensional arrays rely on successfully solving problems such as wiring of elements, electronic and mechanical cross-talk among elements, high impedance of each element and complex multiplexing among elements.

Some techniques have been suggested to reduce the number of the elements of two-dimensional arrays. Sparse arrays, for example, reduce the number of elements by randomly removing elements from periodic dense arrays. However, array performance suffers because of increased sidelobes and loss of gain (Turnbull and Foster 1991). Another way to form a sparce array is to place randomly a fewer number of elements within the array aperture (random position array). This increases the randomness of the array and is expected to reduce the grating lobes, but such arrays may be difficult to construct. In addition, the distance between

some of the elements may be small, which limits the size of these elements and further increases their impedance. To avoid the small interelement distances, one may limit the distance between the centers of any two elements to be greater than a given value. But, as the minimum interelement distance increases, there will be more restrictions on element positioning and thus a reduction in the array randomness.

Electronic sector steering of limited diffraction beams with a two-dimensional array requires that the aperture area loss due to the beam steering should be compensated, so that the cross sections of the beams are always the same (Lu and Greenleaf 1992d). To compensate the aperture, complicated multiplexing of elements is required because the area changes each time a beam is directed to a new direction and there are typically over 100 directions in a scan. A method to reduce to 4 the number of the multiplexing channels in a scan has been suggested (Lu and Greenleaf 1992d). The method divides the scan angle into four ranges, each of which is selected so that the cross section of the beam is approximately the same as that before the steering. A way to avoid the multiplexing of the array elements might be the use of the unsymmetrical limited diffraction beams in eqn (39). One might change the drive functions four times for a rotary symmetric two-dimensional array with different unsymmetrical limited diffraction beams as the beams are steered in the four angle ranges. In this way, the beams would not be destroyed even though the areas of the cross-sections of the beams are reduced and the beams become unsymmetrical. In addition to the beam distortions caused by the area change in a scan, sizes of elements may also cause beam distortions. The grating lobes and FWHM of beams may increase significantly with the size of elements in the scan direction (Lu and Greenleaf 1994).

DISCUSSION

Conventional and limited diffraction beams are usually studied under simplified conditions, *e.g.*, the beams propagate in isotropic-homogeneous and loss-free media without boundaries. In addition we assume that the apertures for limited diffraction beams and Gaussian beams are infinite. These conditions are not satisfied in practice. The following will discuss the influences of some practical conditions on beam forming.

Finite aperture influences

Fluctuation of beams. Limited diffraction beams and Gaussian beams can only be produced with a finite aperture in practice. Therefore, these beams must be truncated with a finite aperture. The truncated beams will be different from the original infinite aperture beams. The depth of field will be reduced and the peak of the beams might fluctuate as they propagate (Durnin et al. 1987). The amplitude of the fluctuation depends on the bandwidth of the beams as well as the ratio of the amplitude of the beams at the truncated edge to the amplitude of the peak of the beams on the aperture. Large fluctuations can cause error in estimation of tissue attenuation if they are not well compensated.

Depth-dependent sidelobes. The resulting sidelobes of limited diffraction beams truncated with a finite aperture will be depth-dependent. The depth-dependent sidelobes may produce noise in the restoration of images if the point spread function of the imaging system is assumed to be depth-independent. However, as the size of the aperture increases, the sidelobes will be less depth-dependent.

Edge waves. Edge waves are produced by the abrupt truncation of the fields of beams on an aperture. The edge waves appear ahead of or behind the main pulses. Their positions and amplitudes are depth-dependent. Because of the depth-dependency, edge waves might also produce noise in an image restoration if they are assumed to be depth-independent. Moreover, the edge waves may produce "ghost" structures in imaging. To reduce the edge waves, aperture apodizations can be used (Lu and Greenleaf 1992a). However, this shortens the depth of field because the effective size of the aperture is reduced. For conventional spherically focused beams, there are no edge waves at the foci because beams from all points on the aperture arrive in phase at the foci. However, the edge waves are present everywhere other than at the foci (Kino 1987; Lu and Greenleaf 1993b).

Other influences

Phase aberration. Phase aberration is a major source of beam distortions. Some biological soft tissues such as the female breasts have strong phase aberration (Foster and Hunt 1979; Trahey et al. 1991). Phase aberration increases with the size of the transducer aperture, central frequency, relative variation of speed of sound (vs. the background) and propagation distance of beams. Various methods for the correction of the phase aberration with array transducers have been proposed (Nock and Trahey 1992; Trahey and Nock 1992; Zhao and Trahey 1991; Fink 1992). However, these methods are compromised by reverberation and nonuniform image brightness. Moving target-based phase aberration correction techniques (Zhao et

Table 1. Summary of principal beam characteristics.

Beams	Aperture weightings (on surface of transducer)	Lateral beamwidth (FWHM)	Depth of field	Phase speed of peak (on axis)
Piston beam (unfocused)	1.0	$\approx 2a$ (in depth of field); $0.71\lambda z/a$ (in far field)	$\pi a^2/\lambda$	c
Piston beam (focused)	$e^{-ik(\sqrt{F^2+r_1^2}-F)}$	$0.71\lambda F/a$ (in focal plane)	Similar to that of focused Gaussian beam	c
Gaussian beam (unfocused)	$e^{-r_1^2/\sigma^2}$	$\approx 1.67\sigma$ (in depth of field); $0.53\lambda z/\sigma$ (in far field)	$\pi\sigma^2/\lambda$	c
Gaussian beam (focused)	$e^{-r_1^2/\sigma^2-ik(\sqrt{F^2+r_1^2}-F)}$	$0.53\lambda F/\sigma$ (in focal plane)	$2\varepsilon F\sqrt{1+2\varepsilon^2}$, where $\varepsilon = \frac{\lambda F}{\pi\sigma^2}$	c
Dynamically focused Gaussian beam	$e^{-r_1^2/\sigma^2-ik(\sqrt{F^2+r_1^2}-F)}(z \equiv F)$	$0.53\lambda F/\sigma$ (for any z)	$F/\sqrt{2}$	c
J_0 Bessel beam	$J_0(\alpha r_1)$	$3.04/\alpha$ (in depth of field)	$a\sqrt{\left(\frac{k}{\alpha}\right)^2 - 1}$	$\frac{c}{\sqrt{1-\left(\frac{\alpha}{k}\right)^2}} > c$
Zero[th]-order X wave (broadband)	$R_e\left\{\frac{a_0}{\sqrt{(r_1 \sin\zeta)^2 + \tau^2}}\right\}$, where $\tau = a_0 + ict$	$2\sqrt{3}a_0/\sin\zeta$ (in depth of field)	$a\cot\zeta$	$\frac{c}{\cos\zeta} > c$
Zero[th]-order X wave (CW)	$J_0(kr_1 \sin\zeta)$	$0.48\lambda/\sin\zeta$ (in depth of field)	$a\cot\zeta$	$\frac{c}{\cos\zeta} > c$
Axicon	1.0	$0.48\lambda/\sin\zeta$ (in depth of field)	Focal zone (see Fig. 6)	$\frac{c}{\cos\zeta} > c$
Ring transducer	$\delta(r_1 - a)$	$0.48\lambda z/a$ (in far field)	$z/\sqrt{2}$	$c/2 + \frac{c}{2}\sqrt{1-\varepsilon^2} < c$, where $\varepsilon = \frac{\sqrt{2}a}{ct}$

λ is the central wavelength; $k = 2\pi/\lambda$ is the wave number; r_1 is the radial distance on transducer surface; a is the radius of the transducer; z is the axial distance; σ is the effective aperture size of a Gaussian beam; F is the focal length; α is the scaling factor of a Bessel beam; ζ is an Axicon angle; and a_0 is the coefficient that determines the fall off rate of the high frequency components of an X wave.

al. 1992) may reduce the influence of the reverberation and nonuniform image brightness, but suffer poor signal-to-noise ratio.

Attenuation. Attenuation of beams in biological soft tissues is frequency dependent and is a function of spatial position. The higher frequency components of a beam have higher attenuation (Wells 1977). This reduces the depth of field (eqn (40)) or resolution (eqn (43)) of limited diffraction beams. Moreover, as more high frequency components are absorbed when the beams propagate deeper into tissues, the beamwidth of the beams may increase with depth (for the Bessel beams, the depth of field, rather than the lateral beamwidth, is dependent of the frequency components (eqn (33)). Spatially dependent attenuation may distort the beams by changing both the phase and amplitude of each plane wave component of the beam.

Anisotropy. An anisotropic medium has a different property for beams propagating in a different direction. According to the spatial Fourier transform (angular spectrum (Goodman 1968)), beams can be expressed as a superposition of plane waves that

propagate in various directions. Therefore, if the media are anisotropic, each plane-wave component of the beams will be modified by different parameters and the desired beams can hardly be constructed.

SUMMARY AND CONCLUSION

Summary

Some of the beams reviewed in this paper are summarized in Table 1, which shows the relationship between lateral beamwidth and depth of field, as well as their relations to beam parameters.

Conclusion

There are an infinity of solutions to the wave equations that produce beams. Beam forming plays an important role in medical imaging and tissue characterization. Beam forming is also applied to other wave-related areas such as nondestructive evaluation of materials, electromagnetics and optics. Conventional spherically focused beams suffer from a short depth of field, but have low sidelobes at their foci. A dynamic focusing technique can be used to increase the depth of field while maintaining low sidelobes. However, when this technique is applied to the transmission of the conventional beams, imaging frame rate is reduced. A special set of solutions to the wave equation, called limited diffraction beams, have a large depth of field and other features that are distinctive from those of conventional beams. They are promising for and might have an impact on beam forming. But these beams have high sidelobes that may lower image contrast. Reduction of the sidelobes of these beams also requires lowering the imaging frame rate or necessitates a wider frequency bandwidth.

Beam forming is governed by the scalar wave equation (for infinite apertures) (eqn (27)) and the Rayleigh–Sommerfeld diffraction formula (for finite apertures) (eqn (1)). These fundamental equations demonstrate that beam forming can only be done in the near field of a transducer. They govern the intrinsic tradeoffs among various imaging requirements, such as lateral and axial resolutions, depth of field, sidelobes, frame rate and system bandwidth. Moreover, beam forming is usually based on the assumption that the media in which beams propagate are isotropic, homogeneous and loss-free. This may not be true in practice, and beam distortion or spreading must be expected.

Among the infinity of solutions to the wave equation exist many beams with special properties that can be selected for specific applications. Certainly these solutions have not been exhaustively searched as yet.

Acknowledgements—The secretarial assistance from Elaine C. Quarve and the graphic assistance from Julie M. Patterson are appreciated. This work was supported in part by grants CA43920 and CA54212 from the National Institutes of Health.

REFERENCES

Bracewell, R. The Fourier transform and its applications. New York: McGraw-Hill Book Company; 1965.

Brittingham, J. B. Focus wave modes in homogeneous Maxwell's equations: Transverse electric mode. J. Appl. Phys. 54:1179–1189; 1983.

Burckhardt, C. B.; Grandchamp, P. A.; Hoffmann, H. Methods for increasing the lateral resolution of B-scan. In: Green, P. S., ed. Acoustical holography. New York: Plenum Press; 1973a: 391–413.

Burckhardt, C. B.; Hoffmann, H.; Grandchamp, P. A. Ultrasound axicon: A device for focusing over a large depth. J. Acoust. Soc. Am. 54:1628–1630; 1973b.

Cai, S. Y.; Bhattacharjee, A.; Marshall, T. C. "Direction-free" optical beams in inverse free electron laser acceleration. In: Nuclear Instruments and Methods in Physics Research, Section A: Accelerators, Spectrometers, Detectors, and Associated Equipment. Proceedings 272:481–484; 1988.

Campbell, J. A.; Soloway, S. Generation of a nondiffracting beam with frequency independent beam width. J. Acoust. Soc. Am. 88:2467–2477; 1990.

Dietz, D. R. Apodized conical focusing for ultrasound imaging. IEEE Trans. Sonics Ultrason. SU-29:128–138; 1982.

Donnelly, R.; Ziolkowski, R. W. A method for constructing solutions of homogeneous partial differential equations: Localized waves. Proc. R. Soc. Lond. A, 437:673–692; 1992.

Donnelly, R.; Ziolkowski, R. W. Designing localized waves. Proc. R. Soc. Lond. A, 440:541–565; 1993.

Donnelly, R.; Power, D.; Templeman, G.; Whalen, A. Graphic simulation of superluminal acoustic localized wave pulses. IEEE Trans. Ultrason. Ferroelec. Freq. Contr. 41:7–12; 1994.

Durnin, J. Exact solutions for nondiffracting beams. I. The scalar theory. J. Opt. Soc. Am. 4:651–654; 1987.

Durnin, J.; Miceli, J. J., Jr.; Eberly, J. H. Diffraction-free beams. Phys. Rev. Lett. 58:1499–1501; 1987.

Evans, D. H.; McDicken, W. N.; Skidmore, R.; Woodcock, J. P. Doppler ultrasound. New York: John Wiley & Sons; 1989: Chapter 4.

Fatemi, M.; Arad, M. A. Ultrasonic nondiffracting beam image formation and restoration. IEEE 1991 Ultrason. Symp. Proc. 91CH3079-1, 2:1305–1308; 1991.

Fatemi, M.; Ahanessians, R. Pulse distortion in nondiffracting beam pulse-echo systems. J. Acoust. Soc. Am. 90(4)Pt. 2:2356; 1991.

Fatemi, M.; Arad, M. A. A novel imaging system based on nondiffracting X waves. IEEE 1992 Ultrason. Symp. Proc. 92CH3118-7, 1:609–612; 1992.

Fink, M. Time reversal of ultrasonic fields—Part I: Basic principles. IEEE Trans. Ultrason. Ferroelec. Freq. Contr. 39:555–566; 1992.

Fishell, E. K.; Foster, F. S.; Connor, T.; Khodai, M.; Harasciewicz, K.; Hunt, J. W. Clinical performance of a cone/annular array ultrasound breast scanner. Ultrasound Med. Biol. 16:361–374; 1990.

Foster, F. S.; Hunt, J. W. The focusing of ultrasound beams through human tissue. In: Metherell, A. F., ed. Acoustical imaging. New York: Plenum Press; 1979: 709–718.

Foster, F. S.; Patterson, M. S.; Arditi, M.; Hunt, J. W. The conical scanner: A two transducer ultrasound scatter imaging technique. Ultrason. Imaging 3:62–82; 1981.

Foster, F. S.; Arditi, M.; Patterson, M. S.; Lee-Chahal, D.; Hunt, J. W. Breast imaging with a conical transducer/annular array hybrid scanner. Ultrasound Med. Biol. 9:151–164; 1983.

Foster, F. S.; Larson, J. D.; Mason, M. K.; Shoup, T. S.; Nelson, G.; Yoshida, H. Development of a 12 element annular array transducer for realtime ultrasound imaging. Ultrasound Med. Biol. 15:649–659; 1989a.

Foster, F. S.; Larson, J. D.; Pittaro, R. J.; Corl, P. D.; Greenstein, A. P.; Lum, P. K. A digital annular array prototype scanner for realtime ultrasound imaging. Ultrasound Med. Biol. 15:661–672; 1989b.

Fujiwara, S. Optical properties of conic surfaces. I. Reflecting cone. J. Opt. Soc. Am. 52:287–292; 1962.

Goodman, J. W. Introduction to Fourier Optics. New York: McGraw-Hill; 1968.

Gori, F.; Guattari, G.; Padovani, C. Model expansion for J_0-correlated Schell-model sources. Optics Comm. 64:311–316; 1987a.

Gori, F.; Guattari, G.; Padovani, C. Bessel-Gaussian beams. Optics Comm. 64:491–495; 1987b.

Gradshteyn, I. S.; Ryzhik, I. M. Table of integrals, series, and products, corrected and enlarged edition. New York: Academic Press; 1980.

Hein, A.; O'Brien, W. D. Current time-domain methods for assessing tissue motion by analysis from reflected ultrasound echoes—A review. IEEE Trans. Ultrason. Ferroelec. Freq. Contr. 40:84–102; 1993.

Hsu, D. K.; Margetan, F. J.; Thompson, D. O. Bessel beam ultrasonic transducer: Fabrication method and experimental results. Appl. Phys. Lett. 55:2066–2068; 1989.

Hunt, J. W.; Arditi, M.; Foster, F. S. Ultrasound transducers for pulse-echo medical imaging. IEEE Trans. Biomed. Eng. BME-30:453–481; 1983.

Indebetow, G. Nondiffracting optical fields: Some remarks on their analysis and synthesis. J. Opt. Soc. Am. A 6:150–152; 1989.

John, F. Partial differential equations. New York: Springer-Verlag; 1982.

Kerr, A. T.; Patterson, M. S.; Foster, F. S.; Hunt, J. W. Speckle reduction in pulse echo imaging using phase insensitive and phase sensitive signal processing techniques. Ultrason. Imaging 8:11–28; 1986.

Kielczynski, P.; Pajewski, W. Application of the transfer function method in calculations of the directivity pattern of ultrasonic transducer. J. Appl. Phys. 70:7257–7260; 1991.

Kino, G. S. Acoustic waves: Devices, imaging, and analog signal processing. Englewood Cliffs, NJ: Prentice-Hall, Inc.; 1987.

Krautkramer, J.; Krautkramer, H. Ultrasonic testing of materials. New York: Springer-Verlag; 1975.

Lin, X. Y.; Zagzebski, J. A.; Boote, E. J. A fast algorithm to calculate ultrasound pressure fields from single-element transducers. IEEE Trans. Ultrason. Ferroelec. Freq. Contr. 36:446–451; 1989.

Lu, J.-Y.; Kinter, T.; Greenleaf, J. F. Measurement and dynamic display of acoustic wave pulses. IEEE 1989 Ultrason. Symp. Proc. 89CH2791-2, 1:673–676; 1989.

Lu, J.-Y.; Greenleaf, J. F. Evaluation of a nondiffracting transducer for tissue characterization. IEEE 1990 Ultrason. Symp. Proc. 90CH2938-9, 2:795–798; 1990a.

Lu, J.-Y.; Greenleaf, J. F. Ultrasonic nondiffracting transducer for medical imaging. IEEE Trans. Ultrason. Ferroelec. Freq. Contr. 37:438–447; 1990b.

Lu, J.-Y.; Kinnick, R.; Greenleaf, J. F.; Sehgal, C. M. Multi-electrical excitation of transducer for ultrasonic imaging. In: Lee, H.; Wade, G., eds. Acoustical imaging. New York: Plenum Press; 1990: 511–519.

Lu, J.-Y.; Greenleaf, J. F. Pulse-echo imaging using a nondiffracting beam transducer. Ultrasound Med. Biol. 17:265–281; 1991a.

Lu, J.-Y.; Greenleaf, J. F. Theory and acoustic experiments of nondiffracting X waves. IEEE 1991 Ultrason. Symp. Proc. 91CH3079-1, 2:1155–1159; 1991b.

Lu, J.-Y.; Greenleaf, J. F. Simulation of imaging contrast of nondiffracting beam transducer. J. Ultrasound Med. 10:S4; 1991c (Abstract).

Lu, J.-Y.; Greenleaf, J. F. Effect on J_0 nondiffracting beam of deleting central elements of J_0 annular array transducer. Ultrason. Imaging 13:203; 1991d (Abs.).

Lu, J.-Y.; Greenleaf, J. F. Nondiffracting X waves—Exact solutions to free-space scalar wave equation and their finite aperture realizations. IEEE Trans. Ultrason. Ferroelec. Freq. Contr. 39:19–31; 1992a.

Lu, J.-Y.; Greenleaf, J. F. Experimental verification of nondiffracting X waves. IEEE Trans. Ultrason. Ferroelec. Freq. Contr. 39:441–446; 1992b.

Lu, J.-Y.; Greenleaf, J. F. Diffraction-limited beams and their applications for ultrasonic imaging and tissue characterization. In: Lizzi, F. L., ed. New developments in ultrasonic transducers and transducer systems. Proc. SPIE 1733:92–119; 1992c.

Lu, J.-Y.; Greenleaf, J. F. Steering of limited diffraction beams with a two-dimensional array transducer. IEEE 1992 Ultrason. Symp. Proc. 92CH3118-7, 1:603–607; 1992d.

Lu, J.-Y.; Greenleaf, J. F. Sidelobe reduction of nondiffracting pulse-echo images by deconvolution. Ultrason. Imaging 14:203; 1992e (Abs.).

Lu, J.-Y.; Greenleaf, J. F. Experiment of imaging contrast of J_0 Bessel nondiffracting beam transducer. J. Ultrasound Med. 11:S43; 1992f (Abs.).

Lu, J.-Y.; Greenleaf, J. F. Producing deep depth of field and depth-independent resolution in NDE with limited diffraction beams. Ultrason. Imaging 15:134–149; 1993a.

Lu, J.-Y.; Greenleaf, J. F. Sidelobe reduction for limited diffraction pulse-echo systems. IEEE Trans. Ultrason. Ferroelec. Freq. Contr. 40:735–746; 1993b.

Lu, J.-Y.; Greenleaf, J. F. A study of sidelobe reduction for limited diffraction beams. IEEE 1993 Ultrason. Symp. Proc. 93CH3301-9. 2:1077–1082; 1993c.

Lu, J.-Y.; Greenleaf, J. F. Formation and propagation of limited diffraction beams. In: Gu, Ben-li, ed. Acoustical imaging. New York: Plenum Press; 331–343; 1993d.

Lu, J.-Y.; Song, T. K.; Kinnick, R. R.; Greenleaf, J. F. *In vitro* and *in vivo* real-time imaging with ultrasonic limited diffraction beams. IEEE Trans. Med. Imag. 12:819–829; 1993.

Lu, J.-Y.; Greenleaf, J. F. A study of two-dimensional array transducers for limited diffraction beams. IEEE Trans. Ultrason. Ferroelec. Freq. Contr. (in press); 1994.

Magnin, P. A. A review of Doppler flow mapping techniques. IEEE 1987 Ultrason. Symp. Proc. 87CH2492-7. 2:969–977; 1987.

McLeod, J. H. The Axicon: a new type of optical element. J. Opt. Soc. Am. 44:592–597; 1954.

Moshfeghi, M. Sidelobe suppression in annular array and axicon imaging systems. J. Acoust. Soc. Am. 83:2202–2209; 1988.

Nock, L. F.; Trahey, G. E. Synthetic receive aperture imaging with phase correction for motion and for tissue inhomogeneities—Part I: Basic principles. IEEE Trans. Ultrason. Ferroelec. Freq. Contr. 39:489–495; 1992.

Ojeda-Castaneda, J.; Noyola-Iglesias, A. Nondiffracting wavefields in grin and free-space. Microwave and Optical Tech. Lett. 3:430–433; 1990.

Oppenheim, A. V.; Schafer, R. W. Digital signal processing. Englewood Cliffs, NJ: Prentice-Hall, Inc.; 1975.

Patterson, M. S.; Foster, F. S.; Lee, D. Sidelobe and speckle reduction for an eight sector conical scanner. IEEE 1981 Ultrason. Symp. Proc. 1:632–637; 1981.

Patterson, M. S.; Foster, F. S. Acoustic fields of conical radiators. IEEE Trans. Sonics Ultrason. SU-29:83–92; 1982.

Smith, S. W.; Pavy, H. E., Jr.; von Ramm, O. T. High-speed ultrasound volumetric imaging system—Part I: Transducer design and beam steering. IEEE Trans. Ultrason. Ferroelec. Freq. Contr. 38:100–108; 1991.

Song, T. K.; Lu, J.-Y.; Greenleaf, J. F. Modified X waves with improved field properties. Ultrason. Imaging 15:36–47; 1993.

Trahey, G. E.; Freiburger, P. D.; Nock, L. F.; Sullivan, D. C. *In vivo* measurements of ultrasonic beam distortion in the breast. Ultrason. Imaging 13:71–90; 1991.

Trahey, G. E.; Nock, L. F. Synthetic receive aperture imaging with phase correction for motion and for tissue inhomogeneities—Part II: Effects of and correction for motion. IEEE Trans. Ultrason. Ferroelec. Freq. Contr. 39:489–495; 1992.

Turnbull, D. H.; Foster, F. S. Beam steering with pulsed two-dimensional transducer arrays. IEEE Trans. Ultrason. Ferroelec. Freq. Contr. 38:320–333; 1991.

Turnbull, D. H.; Foster, F. S. Two-dimensional transducer arrays

for medical ultrasound: Beamforming and imaging. In: Lizzi, F. L., ed. New developments in ultrasonic transducer and transducer system. Proc. SPIE 1733:202–215; 1992a.

Turnbull, D. H.; Foster, F. S. Fabrication and characterization of transducer elements in two-dimensional arrays for medical ultrasound imaging. IEEE Trans. Ultrason. Ferroelec. Freq. Contr. 39:464–475; 1992b.

Uehara, K.; Kikuchi, H. Generation of near diffraction-free laser beams. Appl. Phys. B, 48:125–129; 1989.

Vasara, A.; Turunen, J.; Friberg, A. T. Realization of general nondiffracting beams with computer-generated holograms. J. Opt. Soc. Am. A. 6:1748–1754; 1989.

Vicari, L. Truncation of nondiffracting beams. Optics Comm. 70:263–266; 1989.

Von Ramm, O. T.; Smith, S. W. Beam steering with linear arrays. IEEE Trans. Biomed. Imaging BME-30:438–452; 1983.

Wells, P. N. T. Biomedical ultrasonics. New York: Academic Press; 1977.

Wild, J. P. A new method of image formation with annular apertures and application in radio astronomy. Proc. R. Soc. Lond. A 286:499–509; 1965.

Yamada, K.; Shimizu, H. Conical and toroidal piezoelectric polymer transducers for long range focusing. IEEE Trans. Sonics Ultrason. SU-30:215; 1983.

Zahid, M.; Zubairy, M. S. Directionally of partially coherent Bessel-Gauss beams. Optics Comm. 70:361–364; 1989.

Zhao, D.; Trahey, G. E. Comparisons of image quality factors for phase aberration correction with diffuse and point targets: Theory and experiments. IEEE Trans. Ultrason. Ferroelec. Freq. Contr. 38:125–132; 1991.

Zhao, D.; Bohs, L. N.; Trahey, G. E. Phase aberration correction using echo signals from moving targets I: Description and theory. Ultrason. Imaging 14:97–110; 1992.

Ziolkowski, R. W. Exact solutions of the wave equation with complex source locations. J. Math. Phys. 26:861–863; 1985.

Ziolkowski, R. W. Localized transmission of electromagnetic energy. Phys. Rev. A, 39:2005–2033; 1989.

Ziolkowski, R. W.; Lewis, D. K.; Cook, B. D. Evidence of localized wave transmission. Phys. Rev. Lett. 62:147–150; 1989.

Zou, H.; Lu, J.-Y.; Greenleaf, J. F. Obtaining limited diffraction beams with the wavelet transform. IEEE 1993 Ultrason. Symp. Proc. 93CH3301-9. 2:1087–1090; 1993.